

國立台灣大學理學院海洋研究所

碩士論文

Graduate Institute of Oceanography

College of Science

National Taiwan University

Master Thesis

北南海陸坡海域之第二斜壓模內孤立波

Mode-2 Internal Solitary Wave in the Shelf Break Zone

of northern South China Sea

方盈智

Ying Chih Fang

指導教授：唐存勇 博士

Advisor: Tswen Yung Tang, Ph.D.

中華民國九十六年六月

June, 2007

博碩士論文授權書

(國科會科學技術資料中心版本 93.2.6)

本授權書所授權之論文為本人在 國立台灣 大學(學院) 海洋 系所
物理 組 九十五 學年度第 二 學期取得 碩 士學位之論文。

論文名稱：北南海陸坡海域之第二斜壓模內孤立波

同意 不同意

本人具有著作財產權之論文全文資料，授予行政院國家科學委員會科學技術資料中心(或其改制後之機構)、國家圖書館及本人畢業學校圖書館，得不限地域、時間與次數以微縮、光碟或數位化等各種方式重製後散布發行或上載網路。

本論文為本人向經濟部智慧財產局申請專利(未申請者本條款請不予理會)的附件之一，申請文號為：_____，註明文號者請將全文資料延後半年再公開。

同意 不同意

本人具有著作財產權之論文全文資料，授予教育部指定送繳之圖書館及本人畢業學校圖書館，為學術研究之目的以各種方法重製，或為上述目的再授權他人以各種方法重製，不限地域與時間，惟每人以一份為限。

上述授權內容均無須訂立讓與及授權契約書。依本授權之發行權為非專屬性發行權利。依本授權所為之收錄、重製、發行及學術研發利用均為無償。上述同意與不同意之欄位若未鈎選，本人同意視同授權。

(務必填寫)

研究生簽名：方盈智 (親筆正楷) 學號：R94241103

指導教授姓名：唐存勇 博士

日期：民國 96 年 7 月 16 日

1. 本授權書(得自<http://sticnet.stic.gov.tw/sticweb/html/theses/authorize.html> 下載或至<http://www.stic.gov.tw> 首頁右下方下載)請以黑筆撰寫並影印裝訂於書名頁之次頁。
2. 授權第一項者，請確認學校是否代收，若無者，請個別再寄論文一本至台北市(106-36)和平東路二段106號1702室 國科會科學技術資料中心 黃善平小姐。(本授權書諮詢電話:02-27377606 傳真:02-27377689)

國立臺灣大學碩士學位論文
口試委員會審定書

北南海陸坡海域之第二斜壓模內孤立波
Mode-2 Internal Solitary Wave in the Shelf Break Zone of
Northern South China Sea

本論文係 方盈智 君 (R94241103) 在國立臺灣大學海洋研究所完成之碩士學位論文，於民國 96 年 6 月 4 日承下列考試委員審查通過及口試及格，特此證明

口試委員：(↓欄指導教暫不簽名，待論文修改完成，定稿後再行簽名)

唐存勇 (指導教授)

王曹 吳恩

楊其進

(↓欄待論文修改完成定稿後，先請指導教授簽名，再呈所長簽名)

所長：陳其南

誌謝 (Acknowledgement)

平凡如我，本論文的完成必須感謝太多太多人。首先我要感謝成大棒球校隊，烈日下的揮汗練習以及團隊生活，提供了我身上的磨練，讓我能堅定地解決研究上所遭遇到的困難。謝謝地科 94 級的死黨，你們的關心總是能讓我度過最苦悶的時候。謝謝成大地科系劉正千老師，當年的物理海洋學，把不曉得未來在那的我，引領進這一門美麗的學問，棒球少年的人生就此展開一段不一樣的故事。

台大生活有苦有樂，所上老師的專業使我對海洋有了不一樣的認識。王胄老師和莊文思老師討論時一針見血的見解，總是能直接點明問題的所在，他們同時也是本論文的審核委員，誠摯地感謝他們的寶貴意見。上過陳慶生老師的流體力學後，物理的觀念在清楚的推導下理解，原來這一點都不難。唐老師則提供了絕佳的學習環境，小到上螺絲，大到與外國學者互動，無一不是自己所嚮往的生活，每一刻都是在提升自己，忙雖忙，卻忙得很愉快。

研究室的伙伴陪了我度過這兩年。陳譽愷學長無私的傳承，讓我在寫作程式上奠定了良好的根基，使我有獨立解決問題的能力。瓜哥梁恩昱學長讓我重新拾回對棒球的熱情，研究之餘，每次的投捕練習都是生活上的最佳調劑。楊凱絜學姐則讓我見識到什麼叫做讀書的榜樣，為什麼妳海洋生物能夠考 90 幾分呢？美麗大方的張雅婷學姐不厭其煩地教導我這個大老粗完成每一次的海上任務，雖然總是會有不經意的插曲出現我的生命之中，給學姐添了不少麻煩，也在此特別感謝學姐的包容，讓我在海上學習到更多寶貴的經驗。吳淑芬同學如姐姐般的叮嚀，讓我的生活不至於頹廢到東非原人的地步，咖啡真的蠻好喝的。黃于盈學妹的熱心幫忙，也幫我分擔了不少事情。與樓下彭柏深同學的革命情感，我們陰錯陽差成了麻吉，那段孟不離焦的日子，那段一起當宅男的日子，那段探索台北市的日子，我著實感謝你的出現，我並不孤獨。

學長楊穎堅博士算是這本論文能完成的幕後推手。感謝學長耐心地從無到有教導我，那段從一堆溫度資料抓出訊號的日子總是特別地值得回憶。學長對進度的關心以及對研究態度獨到的見解總是激勵著我不斷前進，每次回家總是得撥一天去跟學長討論心裡才會覺得踏實，一年多過去，糾甘心耶。

戴仁華學長和藹的笑容，總是大方地跟我分享做學問的經驗，程式的寫作上也是惠我良多。熬夜的晚上，總是能聽你述說許多以前的光景，增添我無比的信心，讓我相信這個選擇是對的。也感謝學長在我剛來台大的時候，適時地扮演保母的角色帶領我，我才沒手足無措並開始我的研究。張明輝學長成熟的臉孔下，卻有著比一般人更細膩的思考。由於研究的題材相近，自己也有了一個可以學習的對象，感謝學長慷慨地提供許多研究上的經驗及分析的方法，更是從學長身上學到不少工具的應用。從 Matlab 到 Linux 的 shell script，沒有學長的指導，我不會有現在的功力。

還有太多太多的人，郭怡君同學、符勇慶同學、許庭軒同學、老爹孫漢宗先生、電儀室技正張宏毅先生、賴振哲先生，最帥的錨錠技術員何文華先生，資料庫黃淑貞小姐、詹智丞學長、楊詠甯小姐、劉紹勇先生、賴國榮先生等，海研一號的勇伯、小胖哥等作業人員，工科海洋系李政恩學長、李政則學長、林明宏學長，NPS 的 Dr. Ramp、技術員 Marla、Keith 和 Chris 等人，你們都會在我最需要幫忙的時候出現，還有最美麗的助理楊子萱小姐、徐錦珠小姐張羅大大小小的瑣事，讓我能安心地完成學業。在此由衷地感謝，你們的恩情，在我忘記之前，我是不會忘記的。

最辛苦的莫過於女友幸蓉，當棒球少年轉行變成書呆子，戰場也從紅土變成了大海，一直以來，我似乎只讓她當配角。感謝她為我做出的犧牲以及讓步，讓我可能是全世界有史以來出席率最低的男朋友可以在低潮的時候依靠她這座心靈上的避風港。沒有妳一直的鼓勵和加持，這兩年會比想像中難熬，這得謝誰？真的得謝幸蓉了。

最後，我想謝謝我父母，支持我進入台大這個大家庭，支持我選擇海洋。當然，這一切如果沒有恩師唐存勇老師的提攜，就不會有這麼精彩的兩年。棒球的神啊，雖然我不信你，平凡的我，如果真能對人類做出什麼小小的貢獻，請把成就給我；榮耀請獻給唐存勇老師。

西曆 兩千零七年 仲夏

方盈智

Abstract

A mooring located on the shelf break of northern South China Sea (SCS) measured temperature and current velocity data by thermistor chain and an Acoustic Doppler Current Profiler (ADCP), respectively. Both temperature and current velocity records revealed a number of signals of second baroclinic mode (mode-2) internal solitary wave (ISW), which are seldom observed in nature. Typically, the mode-2 ISWs show the upward/downward displacement of isotherms in the upper/lower water column, respectively. Accordingly, the displacement of isotherms induced by mode-2 ISWs are 33 ± 4 m and 28 ± 4 m in the upper and lower water column, respectively. The characteristic time scale is about 18 minutes as well as the maximum displacement of isotherms is ~ 80 m. The westward propagating mode-2 ISWs emerge generally during the neap tide period. In summer, mode-2 ISWs could have phase-locked with the diurnal tide about 24 hours. In winter, mode-2 ISWs emerge randomly but frequently. The seasonal difference could be associated with the vertical stratification. The thermocline is deeper in winter. Therefore, the water column has one thin layer in middle with temperature varied and two thick layers having near uniform temperature above and below it, respectively. This thermal structure is approximate to a hyperbolic tangent profile, which allows theoretically that a mode-2 ISW propagates along the thermocline with permanent form (Benjamin, 1967 and Davis and Acrivos, 1967, etc). Yang (2007, personal communication) derives a mode-2 ISW analytical solution based on the 3-layer ocean. The solution infers that a high possibility of existence of mode-2 ISWs as long as the middle layer is thin. Therefore, the generation of mode-2 ISW in winter may correlate with the deeper thermocline. Nonetheless, the generating mechanism of mode-2 ISW in summer is different, future studies are needed.

Key words: Internal wave, Solitary wave, mode-2, South China Sea.



摘要

一組分別掛載溫度計串和都普勒流剖儀並施放於北南海陸坡區的錨錠，由其溫度和流速資料發現了為數不少的第二斜壓模之內孤立波。這種形態的內孤立波在自然界中很少被觀測到，一般而言，第二斜壓模之內孤立波會造成等溫面在上部(下部)水層往上(下)的位移。經分析，在上部和下部水層相對應的等溫面位移分別是 33 ± 4 m 和 28 ± 4 m。特徵時間尺度大約是 18 分鐘而其最大振幅可達 80 公尺。波大多往西傳遞且經常在小潮的時候出現。在夏天，第二斜壓模之內孤立波的出現與全日潮有著相位上的一致，約 24 小時。在冬天，第二斜壓模之內孤立波則是隨機且經常性地出現。這種季節上的差異性可能和垂直分層的變化有關。分析冬夏兩季分層的情況可以發現，斜溫層在冬天時比較深。因此，可視為有一層溫度變化的薄層位於上下兩層溫度均的水層之間。這種密度垂直結構近似於雙曲正切函數，理論上可以求得一個在斜溫層傳遞且形狀不變的第二斜壓模之內孤立波的解析解 (Benjamin, 1967 和 Davis and Acrivos, 1967, 等人)。楊(2007)利用三層海洋推導出第二斜壓模之內孤立波的解析解，其結果推論只要中間層為薄層的時候，第二斜壓模之內孤立波就有比較高的機率存在。因此，冬天時第二斜壓模之內孤立波的生成可能與斜溫層比較深有關。然而，夏天時第二斜壓模之內孤立波的生成機制是不相同的，未來仍需要進一步的研究。

關鍵字：內波，孤立波，第二斜壓模，南海。

Contents

I.	Introduction-----	p.9
II.	Analysis and result	
	< A. Field work >-----	p.14
	< B. Observations: a mode-2 ISW event >-----	p.15
	< C. Normal mode analysis >-----	p.16
	<D. The wave-induced isothermal displacement and the characteristic time scale of mode-2 ISWs >-----	p.18
	< E. The propagating direction of mode-2 ISWs >-----	p.21
	< F. Mode-2 ISWs in summer and winter >-----	p.22
	< G. The Difference of the stratification between summer >-----	p.23
III.	Discussion	
	< A. 3-layer ocean >-----	p.41
	< B. “Concave type” mode-2 ISW >-----	p.42
	< C. The influence of the stratification >-----	p.42
	< D. Mode-2 ISW on satellite image >-----	p.44
IV.	Conclusions-----	p.48
	Reference-----	p.50
	Appendix-----	p.53

Table List

TABLE I THE DURATION OF EACH SEGMENT OF THE MOORING S7
-----p.27

TABLE II THE SUMMARY OF THE MOORING S7-----p.27

TABLE III THE TOTAL CASES OF MODE-2 ISWS OBSERVED AT S7
DURING SEGMENT I AND SEGMENT III-----p.31, p.32, p.33



Figure List

- Fig.1** The mode-2 ISW observed in 1999. The top panel is the contour of eastward velocity component (U). The bottom panel is the contour of temperature. (Yang et al., 2004) -----p.13
- Fig.2** Locator map showing the position of the mooring S7.-----p.25
- Fig.3** The design of the mooring S7.-----p.26
- Fig.4** One of mode-2 ISW events observed at S7 during 2005/6/27 10:00 ~ 2005 6/28 10:00 GMT.-----p.28
- Fig.5** The vertical profile of current when a mode-2 ISW passed S7 and the vertical structure (black solid circle line) calculated by normal mode (blue line) --p.29
- Fig.6** The estimated wave-induced isothermal displacement (black solid square line) when a mode-2 ISW passed S7 and the fitted curve (red line).-----p.30
- Fig.7** The histograms of current velocity and direction for mode-2 ISWs observed during segment I at S7.-----p.34
- Fig.8** The histograms of current velocity and direction for mode-2 ISWs observed during segment III at S7.-----p.36
- Fig.9** Depth contours of isotherms from 00:00 GMT, June 22, 2005 to 00:00 GMT, June 30, 2005.-----p.38
- Fig.10** Depth contours of isotherms from 00:00 GMT, December 19, 2005 to 00:00 GMT, December 26, 2005.-----p.39
- Fig.11** **A:** Contours of the buoyancy frequency from 00:00 GMT, June 24, 2005 to 00:00 GMT, June 30, 2005. **B:** Contours of the buoyancy frequency from 00:00 GMT, December 20, 2005 to 00:00 GMT, December 26, 2005.-----p.40
- Fig.12** From left to right is the illustration of a 3-layer ocean, the distribution of the density, and the distribution of the buoyancy frequency.-----p.45

Fig.13 From left to right is the illustration of the mode-2 ISW (usual) and the “concave type” mode-2 ISW.-----p.45

Fig.14 The region of $\alpha_2 > 0$ and $\alpha_2 < 0$ when $\Delta\rho_1 = \Delta\rho_2$ ($\delta=1$)-----p.45

Fig.15 The comparison between the variations of the nonlinearity coefficient of the first two modes in summer and winter, respectively.-----p.46

Fig.16 Satellite image (MODIS) captured a weak ISW-like signal (red ellipse) propagating behind a mode-1 ISWs packet.-----p.47

Fig.17 From left to right is the vertical structure of the vertical velocity and the vertical structure of the horizontal velocity for the motion of mode-2 in a 3-layer ocean.-----p.57



I. Introduction

Internal Solitary Waves (ISWs) are observed in many of the world's marginal seas, straits, fjords, and coastal waters (Fu & Holt, 1982). ISWs are usually evolved from internal tides propagating shoreward or passing a suddenly changed topography. ISWs can propagate for long distance without changing their shape because The nonlinearity balances the dispersion effect. Most of their vertical structures are corresponding to the first baroclinic mode (hereafter referred to as *mode-1* ISWs) (Osborne and Burch, 1980; Fu & Holt, 1982; Ostrovsky and Stepanyants, 1989).

The second or higher baroclinic mode internal solitary wave (hereafter referred to as *mode-2* ISW) is seldom observed in nature. Theoretically, the vertical structures of mode-2 ISWs for the vertical and horizontal velocity have one and two nodal points, respectively. The vertical velocities are opposite above and below the nodal point. Typically, the mode-2 ISWs will induce the upward/downward displacement of isotherms in the upper/lower water column, respectively. The horizontal velocity in between the two nodal points has the same direction as the phase velocity of the wave but has reverse direction with it in above and below the nodal points. Due to the lack of field observations, this phenomenon was first realized in laboratory experiments. Davis & Acrivos (1967) first generated mode-2 ISWs in a water tank with an initial condition as a shallow fluid layer with density varied lying above or below a deep layer with constant density. After intruding some mixed fluid into the layer with density varied, a mode-2 ISW or a 'double-hump' like wave is produced (Davis & Acrivos, 1967; Stamp & Jacka, 1995; Sutherland, 2002). Such waves can propagate along the layer with density varied for a long distance.

Benjamin (1967) obtained a weakly nonlinear analytic solution for the small but finite amplitude mode-2 ISW from an invicid stream function equation (Long,

1953) by assuming a density variation with hyperbolic tangent profile. The solution shows a solitary wave propagating along a thin layer with density varied in an unbounded fluid. Above the middle depth a mode-1 elevation wave is obtained and below the middle depth another depression wave is formed (Benjamin, 1967). The resulting wave has a symmetric ‘bulge’ form about the middle depth and it is the so-called mode-2 ISW analytic solution. However, his solution only applied to the situation with a symmetric density variation about some depth (Tung et al., 1980).

To extend the analytic solution which is only for small but finite amplitude wave, Davis & Acrivos (1967) used the numerical method to examine the solution for arbitrary amplitude waves. They categorized those mode-2 ISWs into “small” amplitude mode-2 ISWs and “large” amplitude mode-2 ISWs. When the ratio of the amplitude of the wave to the thickness of the density varied layer is larger than 1.2, the wave will be classified into “large” amplitude. The numerical result showed that small amplitude mode-2 ISWs with open streamlines can be well described by weakly nonlinear theory. For large amplitude mode-2 ISWs, in the numerical scheme, the streamline near the middle depth bifurcates. This closed streamline region is the result of the diffusion of the vorticity and the effects of viscosity should not be neglected. The analytic solution is invalid (Batchelor, 1956; Davis & Acrivos, 1967; Stamp & Jacka, 1995).

Furthermore, studies on generating mechanism of mode-2 ISWs are notable. Laboratory experiments and numerical simulations show that when mode-1 ISWs are shoaling on the slope and the shelf break, the nonlinearity becomes important, the breaking or the shear instability of mode-1 ISWs could cause strong overturning of the water column and lead to generate mode-2 ISWs (Helfrich & Melville, 1986). Another mechanism is related to an underwater sill. Laboratory and numerical simulations also show that mode-2 ISWs could be generated when the incident

mode-1 wave collides with the underwater sill (Vlasenko & Hutter, 2001; Vlasenko & Alpers, 2005). Baines (1995) showed that the height of the sill and the background current could play an important role on the generation of mode-2 ISWs.

Recently studies indicate that ISWs are active of in northern South China Sea (hereafter referred to as SCS) (Yang et al., 2004, etc). Many ISWs have been observed and studied. Most of them are mode-1 ISWs. It is believed that the mode-1 ISW is primarily generated around Luzon Strait and then propagates to the west. Nonetheless, only some mode-2 ISWs had been recorded and reported. Chang (2001) and Yang et al. (2004) showed a case of mode-2 wave via a moored observation on the shelf break (**Fig.1**). Yang et al. (2004) suggested that the generation of a mode-2 ISW could arise from the barotropic or the mode-1 tidal flow encountering a 3-layer fluid structure which has been observed occasionally and redistributing its energy into the second baroclinic mode. However, the properties of the wave remain mystery.

A long term mooring array is deployed from Luzon Strait to the shelf of the northern SCS under the support of Taiwan/USA joint research program. In this study, a mooring which located on the shelf break is chosen to study the mode-2 ISWs because a number of mode-2 ISWs were seen. It provides a chance to examine the properties of mode-2 ISWs such as amplitude, propagating directions, etc. In section II, field work and observations are introduced. Normal mode methods are used to describe the vertical structures of mode-2 ISWs. The characteristic time scale of mode-2 ISWs is estimated by K-dV equation. Two segments of observations show the differences of appearance between mode-2 ISWs during summer and winter. It is found that the thermocline is deeper in winter. Discussions are in section III. For the 3-layer ocean, a simple theoretical approach is made to discuss the role of the 3-layer ocean and its influence on the resulting mode-2 ISW. The quadratic nonlinearity coefficient of K-dV equation is taken to demonstrate the influence of the stratification.

Conclusions are in section IV..



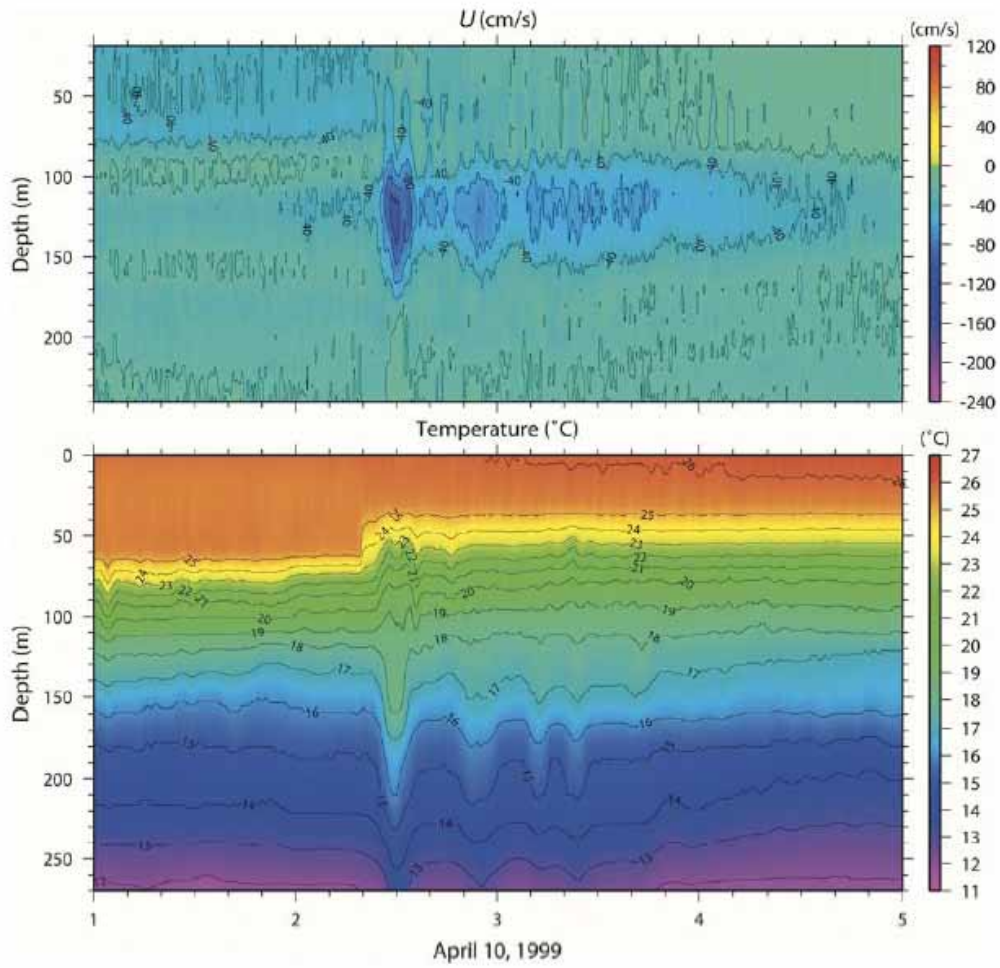


Fig.1 The mode-2 ISW observed in 1999. The top panel is the contour of eastward velocity component (U). The bottom panel is the contour of temperature. (Yang et al, 2004)

II. Analysis and result

< A. Field work >

Under the support of Taiwan/USA joint research programs, Variation around Northern South China Sea/Windy Island Soliton Experiment (VANS/WISE), a mooring array (shown in **Fig.2**) was deployed from Luzon Strait to the shelf of the northern SCS. The data collected at S7, where the water depth is 350m, was chosen study the mode-2 ISW. The mooring was deployed and recovered in April 29, 2005 and June 2, 2006, respectively. 3 times turn-over had been made during this 13 months. Duration can be divided into 4 segments (see **Table I**). The mooring in Segment I and III is designed by Naval Postgraduate School (NPS) while it in Segment II and IV is designed by National Taiwan University (NTU). The diagrams of mooring are shown in **Fig.3**. The latter one has better coverage for the current measurement than the former one, but doesn't have the thermistor chain in the upper water column. Since the temperature measurement is easier to recognize the signal of mode-2 ISWs than current velocity measurement, only the data collected in Segment I and III are used in this study. The NPS mooring has a 300kHz broadband acoustic Doppler current profiler (ADCP) mounted at the 100m depth. The ADCP provided current information from the depth of 15m to 100m. Its bin length was set to 4m. ADCP pinged at 1 second intervals and provided ensemble average every 1 minute. 3 recording current meters (RCM) was below the ADCP, which were mounted at the 160m, 220m and 310m depth, respectively. The RCM provided measurements of deep current every 5 minutes. From top to bottom, a thermistor chain contained temperature pods (T); temperature and pressure sensors (TP); temperature, conductivity, and pressure sensors (TCP) were also mounted on the mooring. The thermistor chain measured samples every 1 minute (TCP at 2 minutes). **Table II**

shows the started and ended times for the two segments and the summary of each instrument.

For the convenience, data from all instruments are interpolated as 1 minute because most instruments provided measurement every 1 minute. It is from 2005/04/29 04:00 to 2005/7/21 14:24 (GMT) in Segment I and from 2005/11/02 04:41 to 2006/02/24 08:33 (GMT) in Segment III. The exceptions are the ADCP and two RCMs in Segment III, they had stopped before 2006/02/24 due to exhaustion of batteries. Data by thermistor chain are used to distinguish signals of mode-2 ISWs. ADCP and three RCMs provide the flow information.

< *B. Observations: a mode-2 ISW event* >

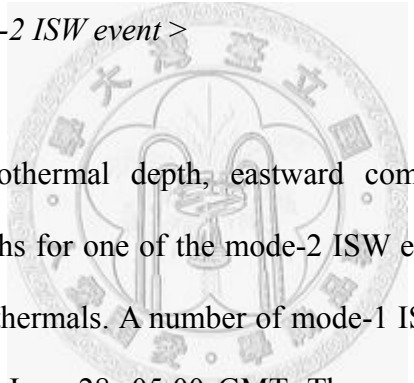


Fig.4 shows the isothermal depth, eastward component velocity (U) and temperature (T) at 12 depths for one of the mode-2 ISW event. The uppermost panel is the depth contour of isothermals. A number of mode-1 ISWs were observed around June 27, 13:00 GMT and June 28, 05:00 GMT. The mode-2 ISW emerged around June 27, 23:30 GMT. A red rectangle marked the mode-2 ISW. The wave had a bulge-like shape which centered around 100m depth. The wave induced isothermal displacement shows an upward displacement above 100m depth and downward displacement below 100m depth. The middle panel displays the contour of eastward velocity component (U). When a mode-2 ISW passed, a westward surge of U occurred between 70m ~ 200m depth. The bottom panel shows the temperature records measured by temperature sensors at different depths. The corresponding depth is shown at the right of the panel. When the mode-2 ISW emerged, it caused a decreasing/increasing temperature fluctuation with amplitude around 3.3 in the upper water column; an increasing/decreasing temperature fluctuation with amplitude

around 2.2 in the upper water column.

< C. Normal mode analysis >

Assuming the internal motion is linear, the displacement η and the horizontal and vertical components of velocity (u, v) and w , respectively, can be separated into vertical and horizontal components. The separation of variables has the form below:

$$\begin{aligned}(u, v) &= \sum_n [u_n(x, y, t), v_n(x, y, t)] q_n F_n(z) \\ w &= \sum_n w_n(x, y, t) W_n(z) \\ \eta &= \sum_n \eta_n(x, y, t) W_n(z)\end{aligned}\tag{1}$$

where F_n and W_n are the vertical modes of horizontal motion and vertical displacement or motion, respectively. q_n is the normalization coefficient for F_n , and u_n , v_n , w_n , and η_n are the corresponding modal coefficient (or amplitude) describing the temporal and horizontal structures. For the internal motion is hydrostatic, frictionless and satisfies the Boussinesq approximation, the vertical modes of vertical displacement or motion are governed by the Sturm-Liouville equation (Gill, 1982):

$$\frac{d^2 W_n(z)}{dz^2} + \frac{N^2(z)}{c_n} W_n(z) = 0\tag{2}$$

and subject to the rigid-lid boundary conditions. Where c_n is the modal phase speed of linear waves, and N is the buoyancy frequency. The buoyancy frequency is defined as follows:

$$N^2 = -\frac{g}{\rho_0} \frac{d\rho}{dz}\tag{3}$$

where ρ_0 is the reference density, ρ is the density and g is the gravitational coefficient. The vertical modes of horizontal and vertical motions are related by:

$$F_n(z) = \frac{dW_n(z)}{dz} \quad (4)$$

The choices for normalization are:

$$\frac{1}{H} \int_{-H}^0 N^2 W_n^2(z) dz = 1$$

$$\frac{1}{H} \int_{-H}^0 F_n^2(z) dz = \frac{1}{q_n^2} \quad (5)$$

where H is local water depth (350m). The theoretical vertical structures can be calculated by **Eqn.(2)** and **Eqn.(4)** based on a buoyancy frequency profile. The buoyancy frequency was estimated by a CTD measurement obtained on 21 April 2005.

The vertical velocity component, w , is estimated from the temperature measurements using temperature conservation equation on the assumption that the nonlinear and horizontal advective are negligible.

$$w(z) = - \frac{\frac{T_t^h(z) - T_{t-\Delta t}^h(z)}{\Delta t}}{\frac{T_t^h(z + \Delta z) - T_t^b(z)}{\Delta z}} \quad (6)$$

where $T_t^h(z)$ and $T_{t-\Delta t}^h(z)$ are the 5-hour high-pass temperature data, $T_t^b(z)$ is the 36-hour low-pass temperature data, z is the depth where the temperature sensor mounted, Δz is the depth difference between two thermistors, t is the time when the mode-2 ISW passed the mooring, and Δt is 1 minutes. Both vertical profiles are taken from the data when a mode-2 ISW passed on June 21, 23:40 GMT, 2005. The background current had been subtracted. The background current is defined as the average of current which was 30 minutes before the arrival of the wave.

In **Fig.5**, the top panel shows $W_2(z)$ (blue line) and the vertical profile of $w(z)$ (black solid circle line) and the bottom panel displays $F_2(z)$ (blue line) and the

vertical profile of $u(z)$ (solid circle line). $W_2(z)$ and $F_2(z)$ are nearly close to the vertical profile of $w(z)$ and $u(z)$, respectively. According to the vertical profile of $w(z)$, the nodal point located around 100m ~ 110m depth while $W_2(z)$ indicated that the nodal point was near 100m depth. w is positive above the nodal point and negative below. In the vertical profile of u , two nodal points located near the depth of 75m and 210m, respectively. $F_2(z)$ showed the zero crossings around the depth of 50m and 230m. u in between the two nodal points was westward but was eastward with it in above and below the nodal point. The vertical profile of v when the mode-2 ISW event passed is not shown here. v is also positive between the two nodal points. However, the amplitude of v is much smaller than u . As mentioned above, the horizontal velocity in between the two points has the same direction as the phase velocity of the wave. It indicated the wave primarily propagated to the west.

< D. The wave-induced isothermal displacement and the characteristic time scale of mode-2 ISWs >

When temperature revealed a decreasing/increasing evolution in the upper water column and an opposite evolution in the lower water column, a mode-2 ISW event is determined. 20 mode-2 ISWs were found during Segment I and 60 mode-2 ISWs were observed during Segment III. Each mode-2 ISW event is catalogued as the time of arrival, the isothermal displacement and the characteristic time scale. The data showed that most mode-2 ISW events had a maximum temperature fluctuation around 75m and 240m, the result is close to the estimate of normal mode analysis. Thus, the isothermal variations at 75m and 240m when a mode-2 ISW passed are used to represent the wave-induced isothermal displacement in the upper and lower water column, respectively.

The wave-induced isothermal displacement is estimated as:

$$\eta_{n,z}(t) \approx \frac{T_t^h(z)}{\frac{T_t^b(z) - T_t^b(z - \Delta z)}{\Delta z}} \quad (7)$$

where T_t^h and T_t^b are the 5-hour high-pass and 36-hour low-pass temperature data, respectively. z is the depth where the temperature sensor mounted(here z is 75m and 240m), Δz is the depth difference between two thermistors. $z - \Delta z$ is 100m and 270m.

According to Lee and Beardsley (1974), Apel et al. (1997) and Apel (2003), the modal expansion in the fundamental hydrodynamics equations, neglecting rotational effects and energy exchange between modes, and assuming weakly nonlinear finite-amplitude plane progressive waves propagating in a specific direction, the modal displacement η_n is governed by the K-dV equation:

$$\frac{\partial \eta_n}{\partial t} + c_n \frac{\partial \eta_n}{\partial x} + \alpha_n \eta_n \frac{\partial \eta_n}{\partial x} + \beta_n \frac{\partial^3 \eta_n}{\partial x^3} = 0 \quad (8)$$

where α_n is the nonlinearity coefficient, β_n is the dispersion coefficient. Both coefficients are also called environmental parameters accounting for conditions like stratification and water depth. They are given by (Vlasenko et al., 2005):

$$\alpha_n = \frac{3}{2Q} c_n \int_{-H}^0 \left(\frac{dW_n(z)}{dz} \right)^3 dz \quad (9)$$

$$\beta_n = \frac{1}{2} \frac{c_n}{Q} \int_{-H}^0 W_n^2(z) dz \quad (10)$$

$$Q = \int_{-H}^0 \left(\frac{dW_n(z)}{dz} \right)^2 dz \quad (11)$$

where Q is the normalization coefficient. If the shallow water approximation holds, the wave-induced isothermal displacement can be described by the solution of the K-dV equation:

$$\eta_n = \eta_{0,n} \operatorname{sech}^2\left(\frac{x - V_n t}{\Delta_n}\right) \quad (12)$$

where η_n is the wave-induced isothermal displacement, $\eta_{0,n}$ is the peak modal amplitude of the solitary wave, t is the time, V_n is the nonlinear phase velocity and Δ_n is the horizontal characteristic length scale. For the mooring observation, the wave-induced isothermal displacement is a function of time, **Eqn.**(12) can be written as:

$$\eta_n = \eta_b + \eta_{0,n} \operatorname{sech}^2(\pi + t^*) \quad (13)$$

η_b is the initial depth of the undisturbed isotherm, t^* is the reference time and τ is related to the characteristic time scale. The characteristic time scale, $T_{c,n}$, is defined as twice the time when the displacement drops to 42% of its peak value. It can be estimated by:

$$T_c = 2\left(\frac{1}{\tau}\right) \quad (14)$$

The isothermal variation at 75m and 240m of all mode-2 ISW events are fitted by using **Eqn.**(13) to estimate the amplitude of wave-induced isothermal displacement $\eta_{0,2,z=75}$ and $\eta_{0,2,z=240}$, respectively. Nonetheless, only the isothermal variation at 75m is used to estimate the characteristic time scale $T_{c,2}$. **Fig.6** is an example. The top panel represents the estimated wave-induced isothermal displacement at 75m (black solid square line) when a mode-2 ISW passed S7 and the fitted line (red line) by using **Eqn.**(13). The bottom panel shows the result at 240m. The mode-2 ISW passed S7 around 03:30 GMT, February 06, 2006.

A threshold of 10m for the amplitude of wave-induced isothermal displacement is used. The calculation of the average amplitude will only include the amplitude above the threshold. It is similar to estimate the average characteristic time scale if the

corresponding amplitude was above the threshold.

In Segment I, the average amplitudes of the wave-induced isothermal displacements are 23 ± 7 m and 30 ± 6 m in the upper and lower water column, respectively. The average characteristic time scale is 18 ± 4 minutes. In Segment III, the average amplitudes of the wave-induced isothermal displacements are 33 ± 4 m and 28 ± 4 m in the upper and lower water column, respectively. The average characteristic time scale is 14 ± 2 minutes. **Table III** shows the summary of each mode-2 event in Segment I and Segment III, respectively.

< E. The propagating direction of mode-2 ISWs >

The analysis can be made using a RCM which is located at 160m depth. For most mode-2 ISWs, nodal points of the horizontal velocity component are located above 160m and below, respectively. Thus, the current at the 160m depth is used to determine the direction of the wave in this study. When mode-2 ISW passed by the mooring, the current at the half time of the wave's passage is used. The background current has been subtracted. The background current is defined as the average of current which was 30 minutes before the arrival of the wave. **Fig.7** shows the histograms of current speed and propagating direction for mode-2 ISWs observed during segment I at S7. The upper panel is the rose diagram. The angle histogram shows the distributions of current at 160m depth. The different colors are indicated the different cases of mode-2 ISW events. The distributions of current are split into 16 groups from $0 \sim 2\pi$. The azimuth 0° (or 360°) shows the east, 90° is the north, 180° is the west and 270° represents the south. The lower panel is the histogram of current speed. Each bar shows the wave with that current speed, which is denotes on the x-axis. The length of the bar indicates the number of appearance. **Fig.8** is similar as

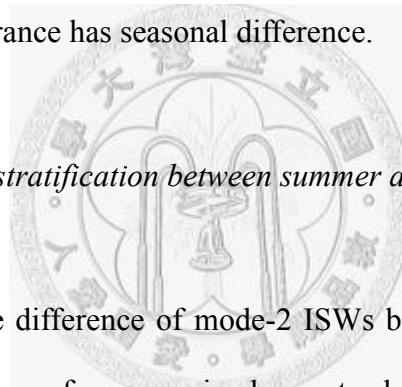
Fig.7 but for Segment III. It is apparent from **Fig.7** and **Fig.8** to see that westward propagating mode-2 ISWs were prevailing. Some waves seemed to be reflected wave because they propagated to the east. The data also indicates that mode-2 ISWs were frequently observed during segment III. It is worthy to note that segment I was during summer and segment III was during winter. Thus, mode-2 ISWs emerged more frequently in winter than in summer.

< F. Mode-2 ISWs in summer and winter >

In summer, **Fig.9** shows depth contours of isotherms on S7. The x-axis denotes the time and y-axis denotes the water depth. From top to bottom there are 8 panels. Each panel represents one day (June 24 ~ July 04, 2005) from 00:00 to 24:00. In the left part of each panel is the date. The black rectangle indicates the mode-2 ISW. According to previous observations (Ramp et al., 2004), mode-1 ISW packets emerged twice each day in this mooring site. It also indicated two mode-1 ISW packets passed S7 each day. Both mode-1 ISW packets arrived S7 about 1 hour later each day. It infers that the M2 tide could be dominant to generating those waves. It is interesting that the mode-2 ISW (shown in the black rectangle) appeared regularly and seemed phase-locked to the diurnal tide about 24 hours. The emergence of mode-2 ISW was once every day around 23:30 GMT from June 24 to June 27, except one mode-2 ISW event appeared around June 24, 00:00 GMT. After June 29, the mode-1 ISW seemed to be disappeared. However, two mode-2 ISW events appeared around July 1, 16:00 GMT and July 4, 23:00 GMT. It could be inferred that the emergence of mode-2 ISW seemed to be once each day. It suggests that mode-2 ISWs could be related by the diurnal tide.

Fig.10 is similar as **Fig.9** but for winter. From top to bottom there are 13 panels.

Each panel represents one day (December 19 ~ 31, 2005) from 00:00 to 24:00. In the left part of each panel is the date and the number in parenthesis means the date on the lunar calendar. The black rectangle indicates the mode-2 ISW. The contour of temperature shows a different condition in winter. No apparent mode-1 ISWs appeared regularly except several short-wavelength elevation mode-1 ISW-like waves emerged behind the mode-2 ISW. More than 20 mode-2 ISW emerged in 13 days. The most remarkable feature is that mode-2 ISWs appeared randomly but frequently. Some mode-2 ISWs revealed as a series of 2 or 3 waves. The random appearance indicates the waves could be generated locally. To summarize briefly the observations of mode-2 ISW in summer and winter, most mode-2 ISW appeared during the neap tide period but their appearance has seasonal difference.



< G. The Difference of the stratification between summer and winter >

In order to study the difference of mode-2 ISWs between summer and winter, the variation of the buoyancy frequency is chosen to demonstrate the difference of stratification as mode-2 ISWs appeared. It can be estimated by the temperature time series data and using **Equ.(3)**. The vertical profile of ρ is estimated by the temperature data provided by thermistor chain and assuming the salinity = 35.00 psu.

For summer, **Fig.11A** shows contours of the buoyancy frequency. The x-axis denotes the time and y-axis denotes the water depth. The colorbar indicates that the large N^2 is colored in green to red. The large buoyancy frequency can be considered the thermocline (or the pycnocline). If the water is uniform, the buoyancy frequency will be small and the color will be close to blue. From top to bottom there are 6 panels. Each panel represents one day (June 24 ~ 29, 2005) from 00:00 to 24:00. **Fig.11B** is similar as **Fig.11A** but for winter. From top to there are also 6 panels. Each panel

represents one day (December 20 ~ 25, 2005) from 00:00 to 24:00. In **Fig.11A**, the thermocline located around 80m ~ 100m depth. In **Fig.11B**, the thermocline was deeper, especially on the second and third panel, it presents that the thermocline located near 200m depth. It is apparent to see that the stratification is different between summer and winter. The thermocline is deeper in winter. As the thermocline was deep, mode-2 ISWs emerged more frequently while mode-1 ISWs were vague. It infers that a deeper thermocline could be favorable for the generation of mode-2 ISW. Further discuss will be in next section.



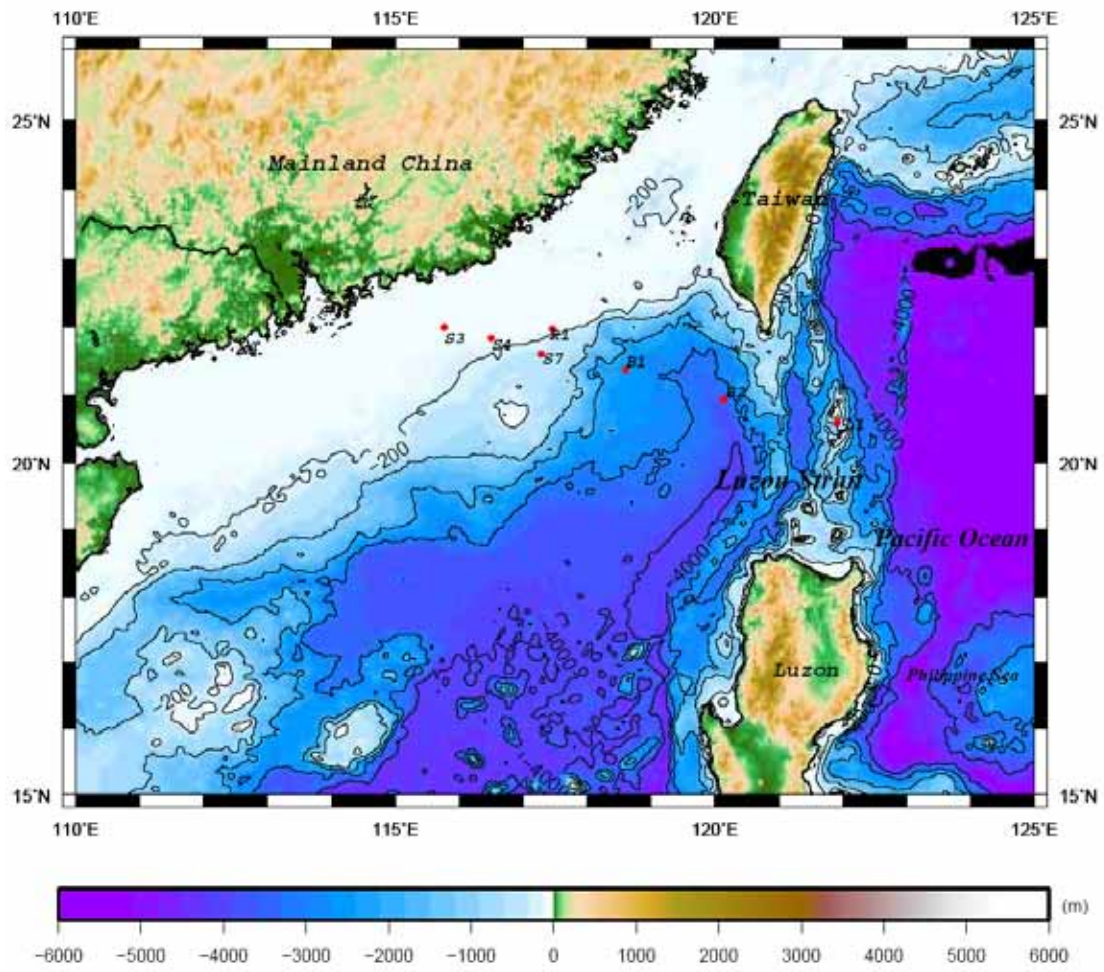


Fig.2 Locator map showing the position of the mooring array of VANS/WISE.

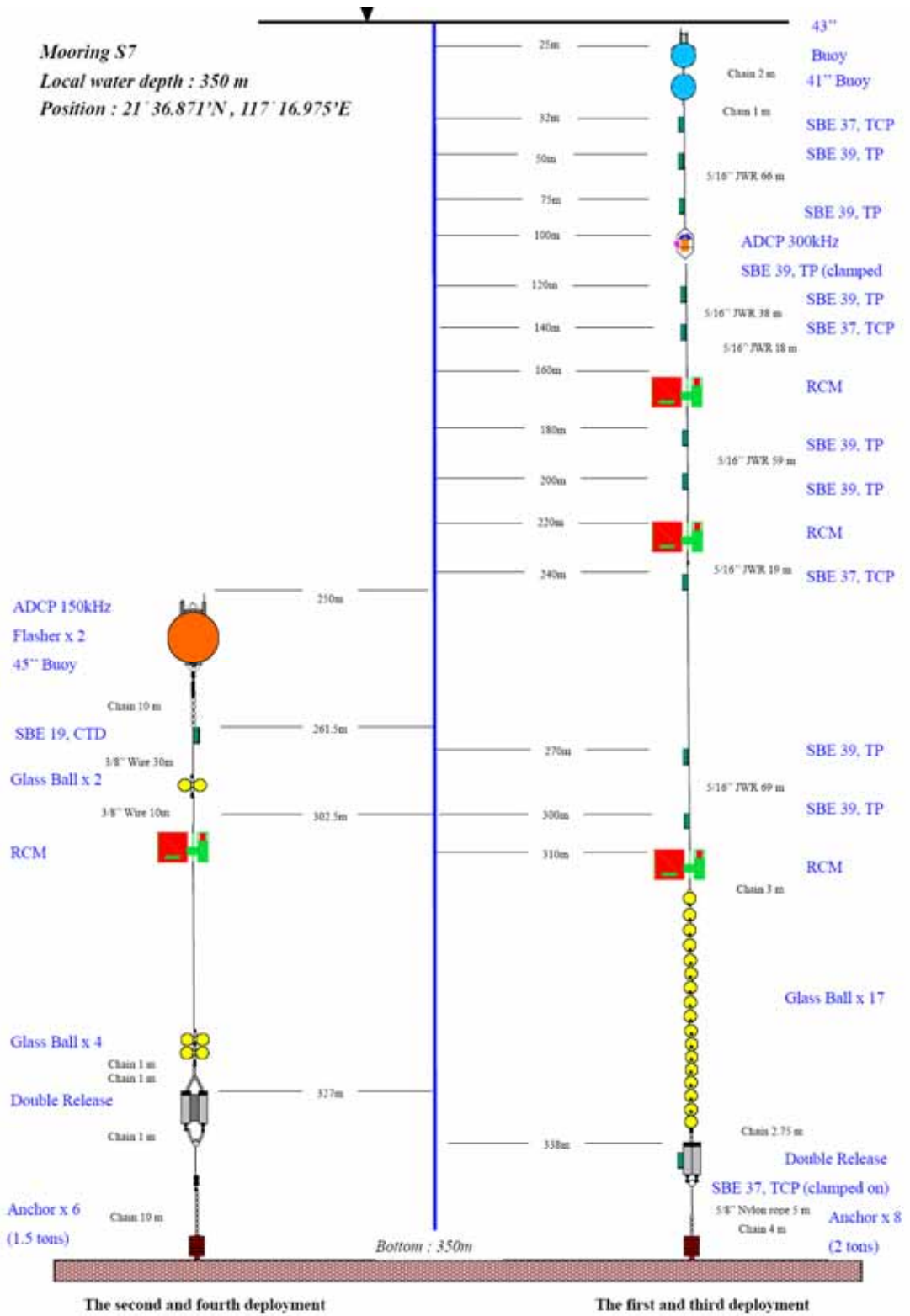


Fig.3 The design of the mooring S7.

TABLE I
THE DURATION OF EACH SEGMENT OF THE MOORING S7

	Segment I	Segment II	Segment III	Segment IV
Start	2005/04/29	2005/07/28	2005/11/02	2006/02/24
End	2005/07/28	2005/11/01	2006/02/24	2006/06/02

TABLE II
THE SUMMARY OF THE MOORING S7

Instrument Depth (m)	Instrument	Data Duration Segment I	Data Duration Segment III	Sampling rate (min)	ADCP Recording Depth (m)
32	TCP	2005/4/29~2005/07/21	2005/11/02~2006/02/24	2	15~100, bin length : 4
50	TP	2005/4/29~2005/07/21	2005/11/02~2006/02/24	1	
75	TP	2005/4/29~2005/07/21	2005/11/02~2006/02/24	1	
100	TP	2005/4/29~2005/07/21	2005/11/02~2006/02/24	1	
100	ADCP, 300kHz	2005/4/29~2005/07/21	2005/11/02~2006/01/18	1	
120	TP	2005/4/29~2005/07/21	2005/11/02~2006/02/24	1	
140	TCP	2005/4/29~2005/07/21	2005/11/02~2006/02/24	2	
160	RCM	2005/4/29~2005/07/21	2005/11/02~2006/02/21	5	
180	TP	2005/4/29~2005/07/21	2005/11/02~2006/02/24	1	
200	TP	2005/4/29~2005/07/21	2005/11/02~2006/02/24	1	
220	RCM	2005/4/29~2005/07/21	2005/11/02~2006/02/21	5	
240	TCP	2005/4/29~2005/07/21	2005/11/02~2006/02/24	2	
270	T	2005/4/29~2005/07/21	2005/11/02~2006/02/24	1	
300	TP	2005/4/29~2005/07/21	2005/11/02~2006/02/24	1	
310	RCM	2005/4/29~2005/07/21	2005/11/02~2006/02/21	5	
338	TCP	2005/4/29~2005/07/21	2005/11/02~2006/02/24	2	

T: Temperature sensors
 TP: Temperature and Pressure sensors
 TCP: Temperature, Conductivity, and Pressure sensors
 ADCP: Acoustic Doppler Current Profiler
 RCM: Rotary Current Meter

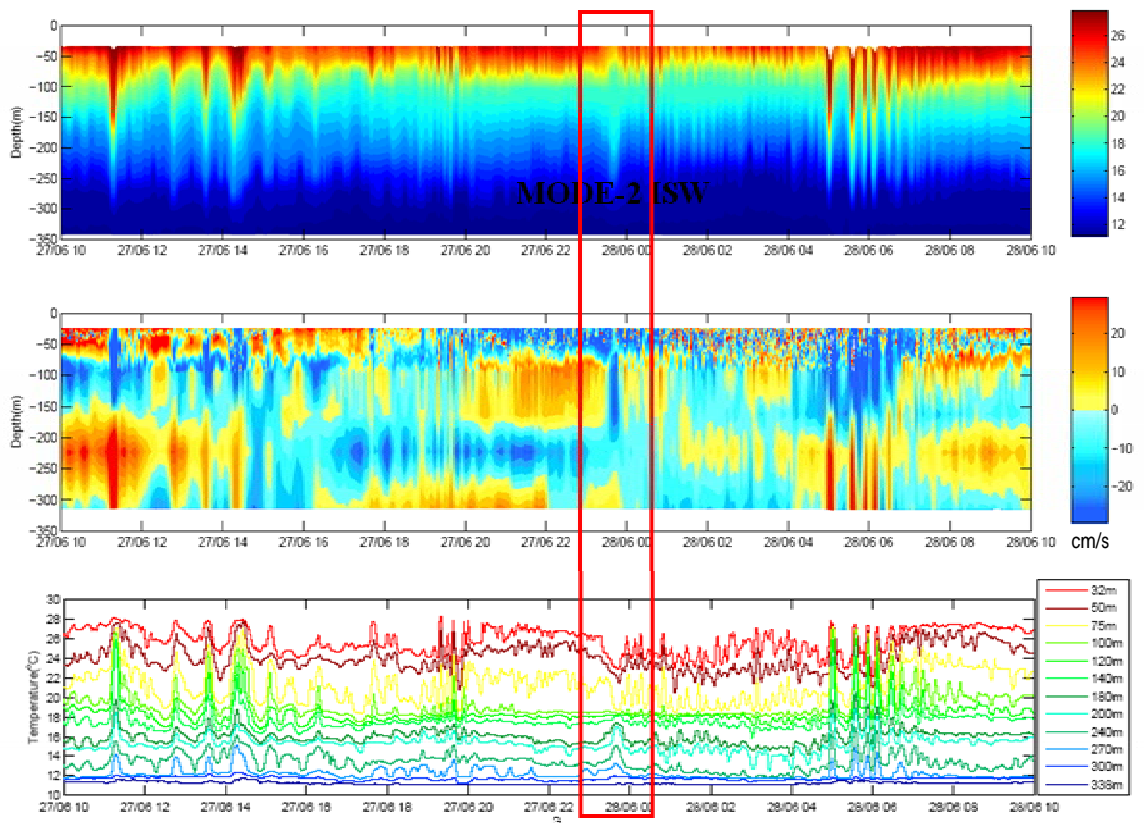


Fig.4 One of the mode-2 ISW event which was passing by S7 during 2005/6/27 10:00 ~ 2005 6/28 10:00 GMT. From top to bottom: the first panel is the depth contour of isotherms; the second panel is the contour of eastward velocity component (U); the third panel is the time series of temperature.

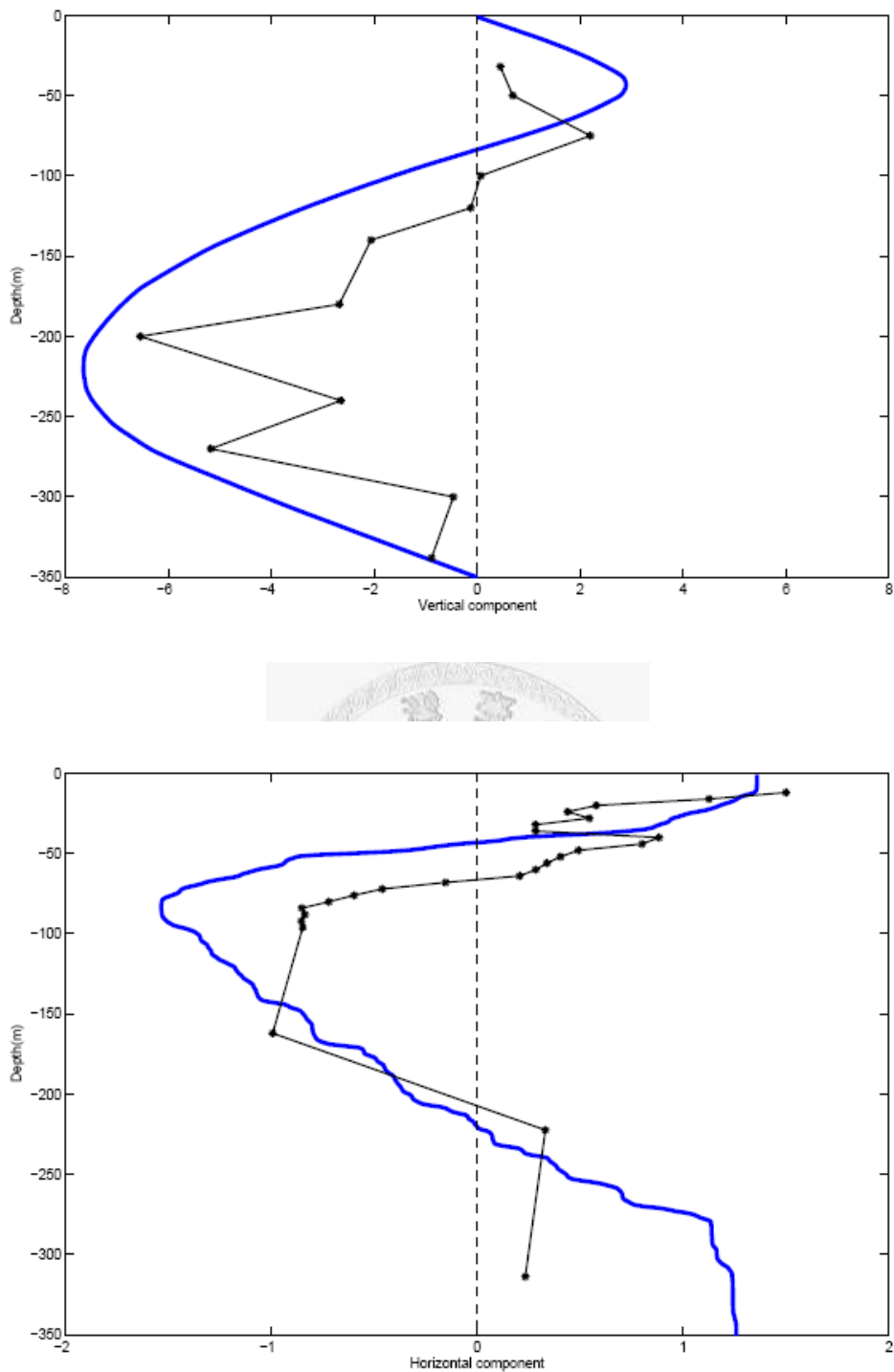
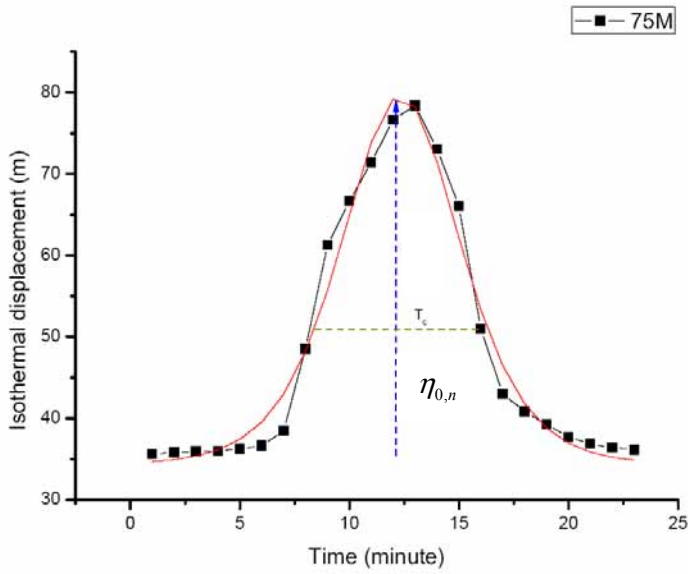


Fig.5 The top panel shows $W_2(z)$ (blue line) and the vertical profile of w (black solid circle line) while the bottom panel displays $F_2(z)$ (blue line) and the vertical profile of u (solid circle line). Both vertical profiles are taken from the data when a mode-2 ISW passed on June 21, 23:40 GMT, 2005. The background current had been subtracted.



FITTED CURVE: $\eta_n = \eta_b + \eta_{0,n} \operatorname{sech}^2(\alpha + t^*)$, $T_c = 2\left(\frac{1}{\alpha}\right)$

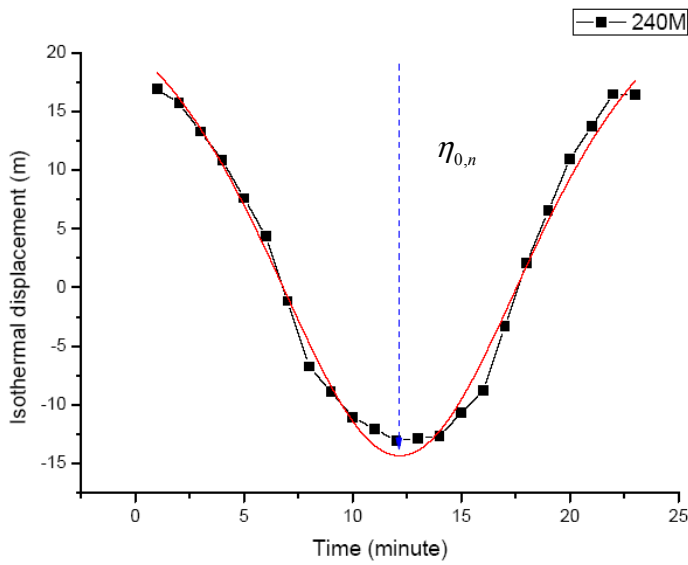


Fig.6 The top panel represents the estimated wave-induced isothermal displacement at 75m (black solid square line) when a mode-2 ISW passed S7 and the fitted curve (red line) by using **Eqn.**(13). The bottom panel shows the result at 240m. The mode-2 ISW passed S7 around 03:30 GMT, February 06, 2006.

TABLE III
 THE TOTAL CASES OF MODE-2 ISWS OBSERVED AT S7
 DURING SEGMENT I AND SEGMENT III

Segment I	Δm	Δm	
Mode-2 Event	Isothermal displacement	Isothermal displacement	Characristic Time Scale
yymmdd, hh	(at 75m)	(at 240m)	Minutes
050503, 04	37	38	29
050504, 10	28	11	12
050522, 06	10	9	20
050525, 03	11	3	5
050602, 14	7	6	11
050610, 01	19	42	15
050619, 01	4	6	13
050619, 03	11	5	14
050619, 04	11	17	16
050622, 23	18	19	10
050624, 00	23	23	24
050624, 23	49	48	20
050625, 03	30	35	27
050625, 23	14	30	6
050626, 00	X	30	30
050627, 23	2	30	7
050701, 17	53	20	31
050705, 23	7	1	3
050706, 21	21	43	12
050709, 21	21	28	14

Segment III			
Mode-2 Event yymmdd, hh	Δm	Δm	Characristic Time Scale Minutes
	Isothermal displacement (at 75m)	Isothermal displacement (at 240m)	
051107, 11	23	45	19
051109, 13	25	3	31
051110, 13	12	19	12
051112, 17	38	17	9
051113, 16	43	46	14
051114, 17	25	18	9
051118, 04	12	51	10
051118, 05	25	10	9
051120, 04	41	10	7
051120, 06	24	20	7
051122, 09	21	13	6
051124, 05	2	11	8
051125, 11	16	16	30
051127, 05	12	17	8
051129, 21	36	11	19
051130, 08	3	17	8
051102, 08	6	26	10
051203, 07	54	13	9
051203, 10	22	16	6
051205, 11	30	7	8
051205, 11	39	29	36
051206, 07	35	40	8
051221, 08	24	16	7
051221, 09	26	37	11
051221, 11	X	61	14
051222, 01	X	50	27
051222, 01	1	47	27
051224, 06	2	31	6
051224, 16	48	51	9
051225, 08	22	34	7
051225, 08	6	23	9
051225, 09	14	19	6
051225, 16	29	40	10
051225, 16	22	28	13
051226, 16	30	65	29
051226, 18	20	45	8
051227, 10	37	40	14
051229, 11	25	21	16
051230, 11	42	14	13
051231, 01	51	16	8
051231, 08	17	18	8
060105, 04	10	13	31
060119, 10	19	29	33

060129, 03	20	29	29
060206, 03	45	42	7
060206, 04	45	39	6
060206, 19	58	2	40
060209, 23	10	4	6
060213, 01	15	15	5
060214, 07	63	3	16
060215, 07	54	13	6
060215, 08	68	10	10
060219, 01	29	32	20
060221, 23	55	10	26
060222, 05	43	13	16
060223, 00	29	38	14
060223, 01	53	65	10
060223, 06	80	43	10
060204, 00	57	21	4



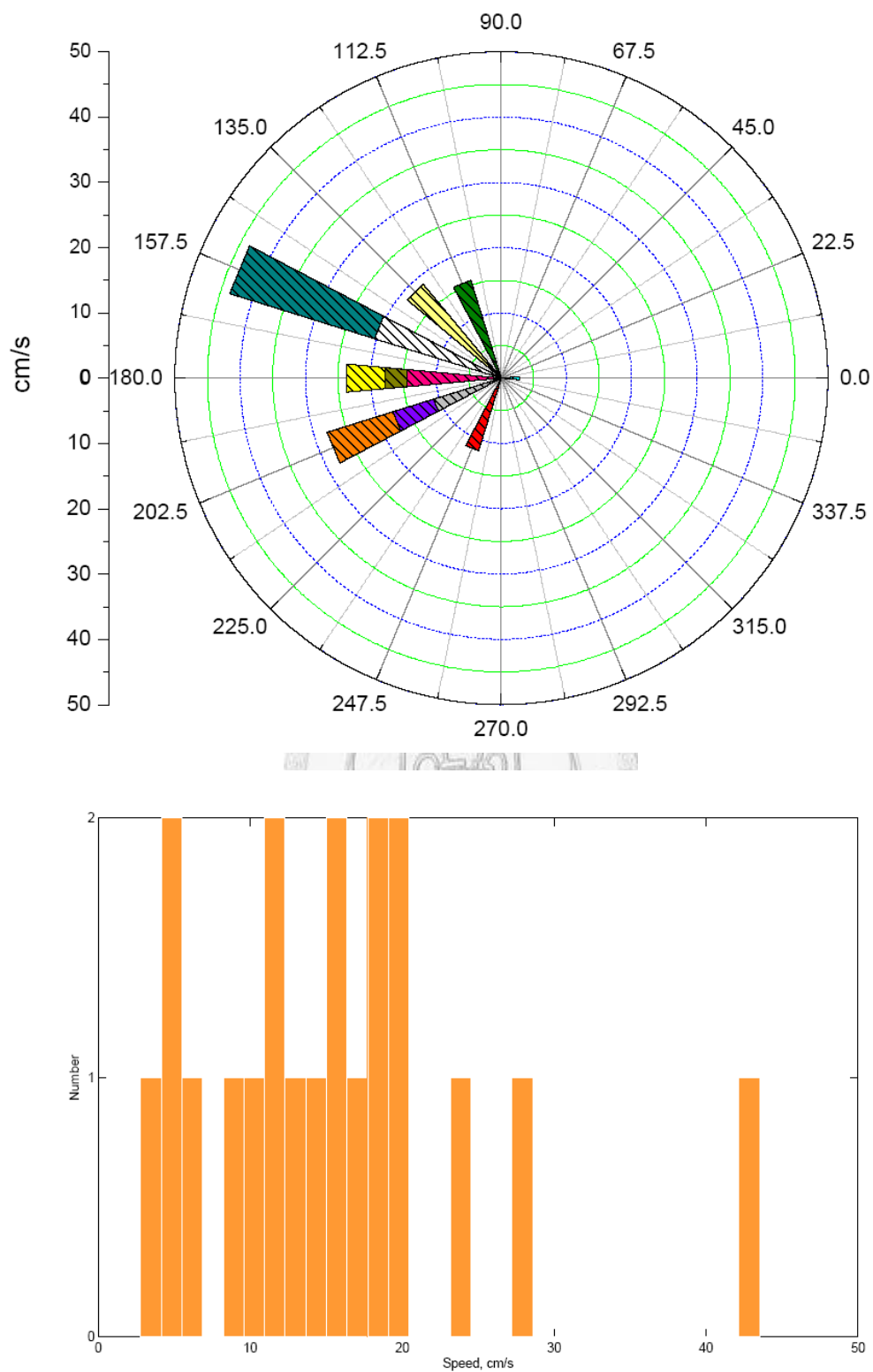


Fig.7 The histograms of current speed and propagating direction for mode-2 ISWs observed during segment I at S7. The upper panel is the rose diagram. The different colors are indicated the different cases of mode-2 ISW events. The distributions of

current are split into 16 groups from $0 \sim 2\pi$. The azimuth 0° (or 360°) shows the east, 90° is the north, 180° is the west and 270° represents the south. The lower panel is the histogram of current speed. Each bar shows the wave with that current speed, which is denoted on the x-axis. The length of the bar indicates the number of appearance.



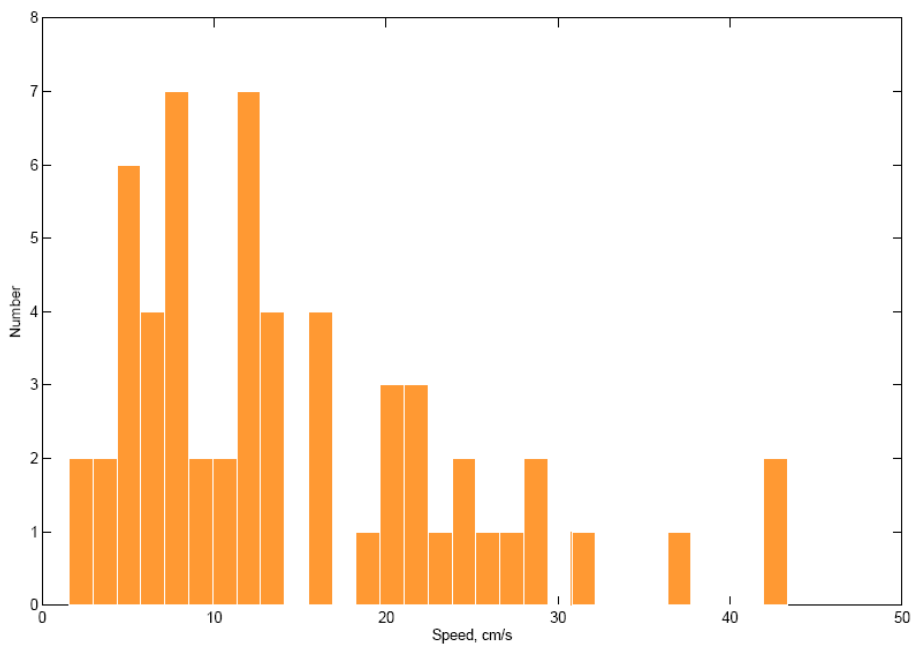
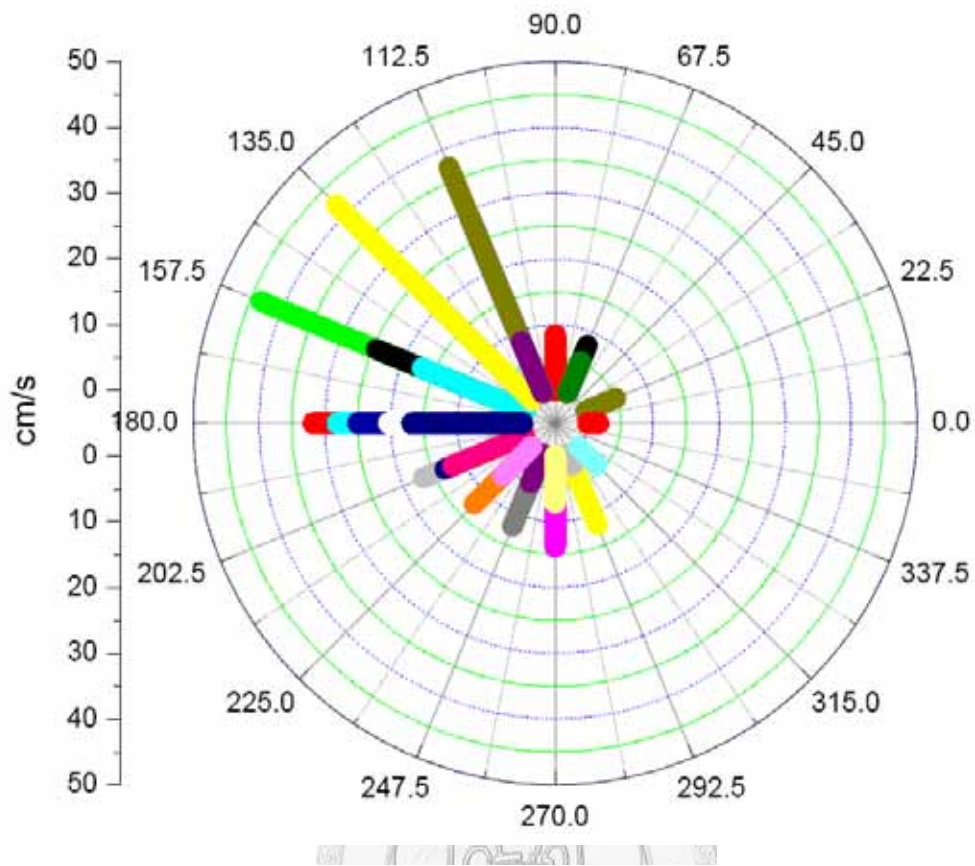


Fig.8 The histograms of current speed and propagating direction for mode-2 ISWs observed during segment III at S7. The upper panel is the rose diagram. The different colors are indicated the different cases of mode-2 ISW events. The distributions of

current are split into 16 groups from $0 \sim 2\pi$. The azimuth 0° (or 360°) shows the east, 90° is the north, 180° is the west and 270° represents the south. The lower panel is the histogram of current speed. Each bar shows the wave with that current speed, which is denoted on the x-axis. The length of the bar indicates the number of appearance.



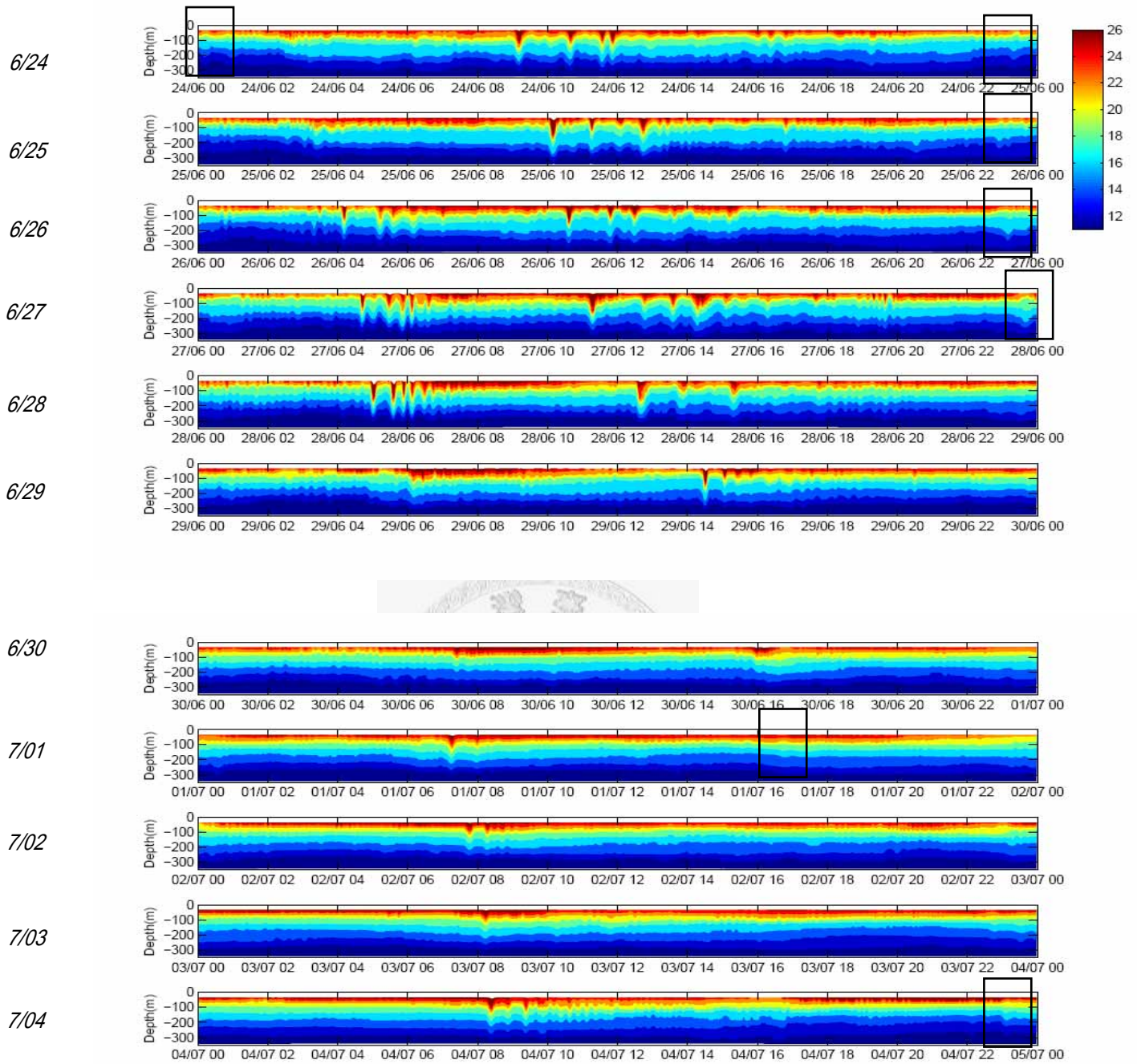


Fig.9 Depth contours of isotherms from 00:00 GMT, June 22, 2005 to 00:00 GMT, June 30, 2005. From top to bottom there are 8 panels and each panel represents 1 day. In the left part of each panel is the date. The black rectangle indicates the mode-2 ISW.

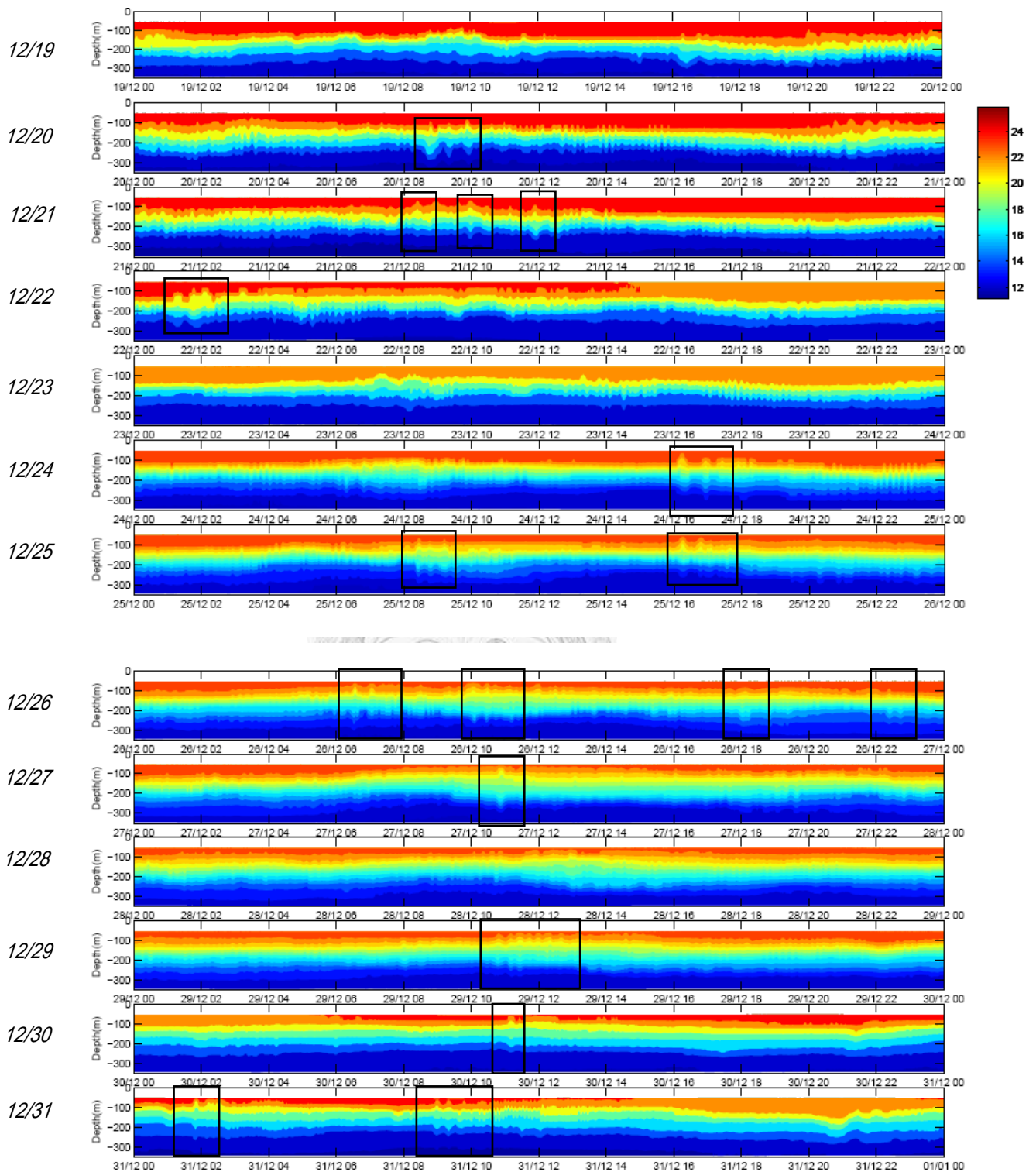
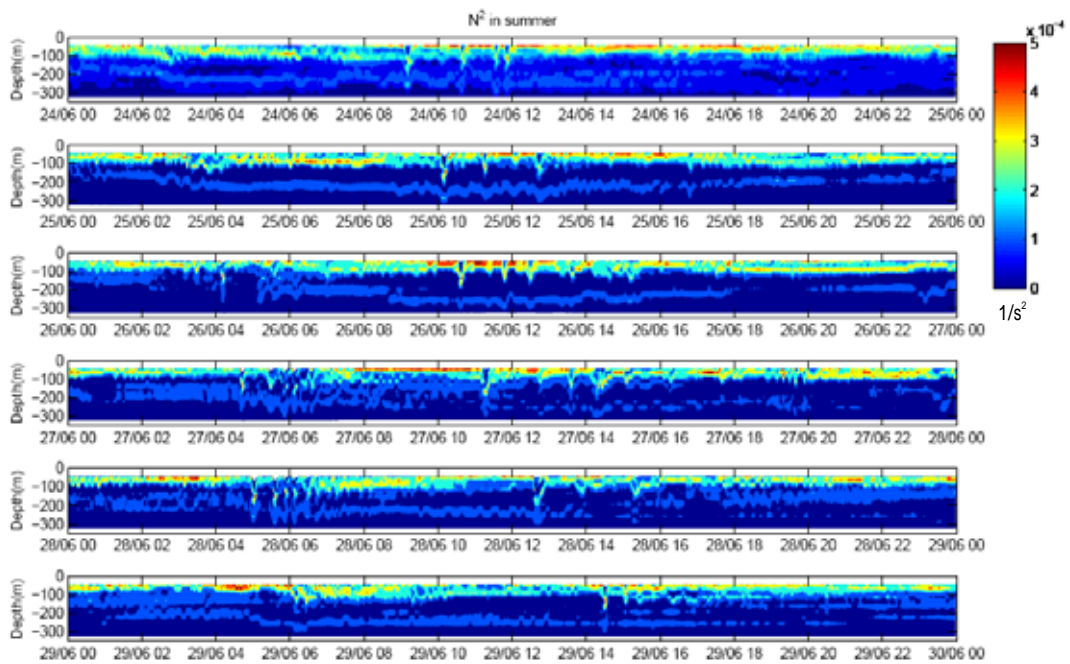


Fig.10 Depth contours of isotherms from 00:00 GMT, December 19, 2005 to 00:00 GMT, December 31, 2005. From top to bottom there are 13 panels and each panel represents 1 day. In the left part of each panel is the date. The black rectangle indicates the mode-2 ISW

A. Summer



B. Winter

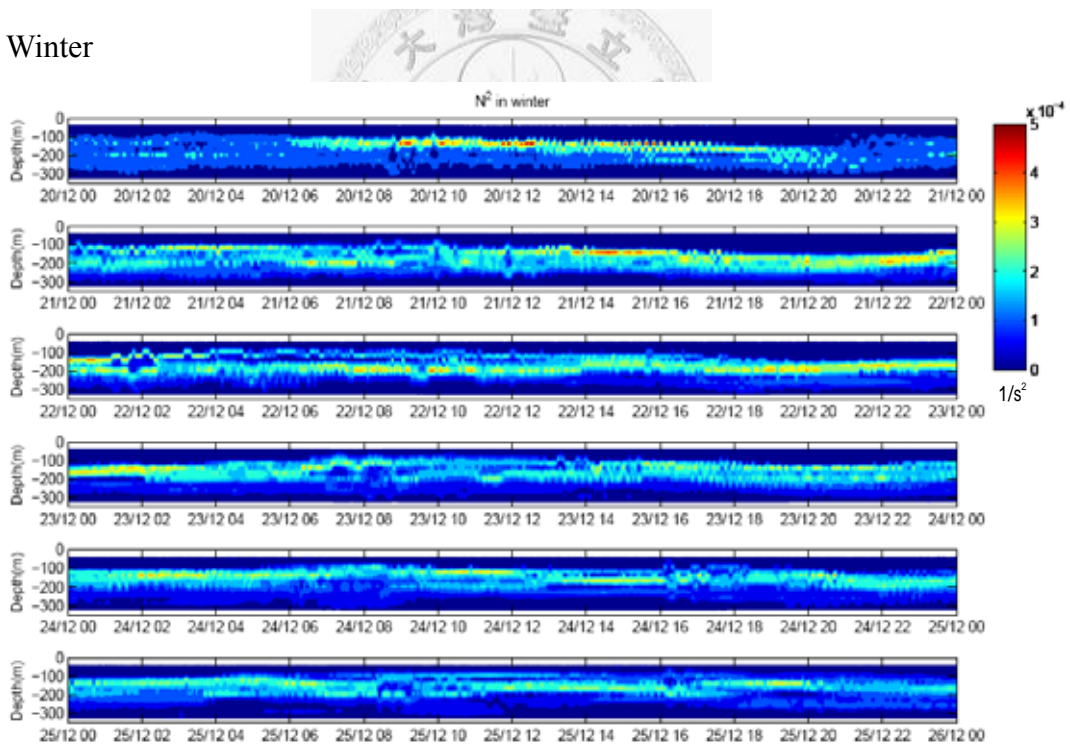


Fig.11 A: Contours of the buoyancy frequency from 00:00 GMT, June 24, 2005 to 00:00 GMT, June 30, 2005. From top to bottom there are 6 panels and each panel represent 1 day. B: Contours of the buoyancy frequency from 00:00 GMT, December 20, 2005 to 00:00 GMT, December 26, 2005. From top to bottom there are 6 panels and each panel represent 1 day.

III. Discussion

< A. 3-layer ocean >

A simple 3-layer ocean (**Fig.12**) is used to demonstrate the role of the 3-layer ocean and its influence on the resulting mode-2 ISW (Yang, 2007, personal communication). Each layer has its individual density, the vertical structure of vertical velocity $W(z)$ can be expressed by **Eqn.(2)**. In the 3-layer ocean with a solid bottom, using the rigid lid approximation, it assumes there is a vertical velocity at the interface. The degree of freedom of the 3-layer ocean is 2. Thus, a mode-2 solution can be obtained by letting the vertical velocity at the two interfaces be different signs. As mentioned in chapter II, the modal displacement η_n is governed by the KdV equation (**Eqn.(8)**)

In the mode-1 condition, if $c_1 > 0$ which indicates a solitary wave propagating to the positive x-axis, it can conclude that the sign of η_1 and α_1 are the same. When $\alpha_1 > 0$, $\eta_1 > 0$ which is an elevation solitary wave. When $\alpha_1 < 0$, $\eta_1 < 0$ which is a depression solitary wave. In addition, in the mode-2 condition, when $\alpha_2 > 0$, it will be $\eta_2 > 0$ above the nodal point of the vertical velocity and $\eta_2 < 0$ below the nodal point. The shape of the wave is the same as the one observed in the northern SCS (appendix). α_2 is also the function of the thickness of each layer in the 3-layer ocean. **Fig.13** shows the region of $\alpha_2 > 0$ and $\alpha_2 < 0$ when the density difference is the same between each layer in the 3-layer ocean. The x axis represents the percentage of the thickness of the upper layer h_1 of the total water depth ($H=h_1+h_2+h_3$). The y axis represents the percentage of the thickness of the intermediate layer h_2 of the total water depth ($H=h_1+h_2+h_3$). The result infers a high possibility that a mode-2 ISW could also exist in case the thickness of the intermediate layer is less than 50% of water depth. It is also coincident with many laboratory experiments whose initial condition is a thin layer in middle. Detailed derivations are in appendix.

Nevertheless, it is difficult to make a pure 3-layer environment in laboratory. The fluid will diffuse and cause leakage. This diffusive process may smooth the density variation. Accordingly, the intermediate layer would become density varied. The stratification is approximate to that with a deep thermocline in winter. From **Fig.9B**, mode-2 ISWs appeared frequently in winter, the estimated thickness of the

thermocline (or pycnocline) in winter is about 100m. It is about 29% to the total water depth and agrees with the predictions of the 3-layer ocean.

< B. “Concave type” mode-2 ISW >

Another analytic solution of the 3-layer ocean predicts another type of mode-2 ISW. When $\alpha_2 < 0$, it will be $\eta_2 < 0$ above the nodal point of the vertical velocity and $\eta_2 > 0$ below the nodal point. According to the shape of the wave, it was preliminary called “concave type” mode-2 ISW (Yang, 2007, personal communication). In order to divide mode-2 ISW which was commonly seen in SCS, the common type of mode-2 ISW is termed “usual” mode-2 ISW. “Concave type” mode-2 ISW is not yet confirmed by theories and experiments. In **Fig.12**, “concave type” mode-2 ISW occurs in the region of $\alpha_2 < 0$. The result suggests that a “concave type” mode-2 ISW could exist in case the thickness of the middle layer is more than 50% of water depth. However, the stratification with a thick layer in middle is seldom in the ocean. Therefore, “concave type” mode-2 ISW could be in existence under very unique stratification. The illustration is shown in **Fig.14**.

Total of 80 usual mode-2 ISW events were observed. However, only 6 cases were suspected to “concave type” mode-2 ISW. The number is too few to verify its existence in the ocean. Future study is required.

< C. The influence of the stratification >

In the 3-layer ocean, the nonlinearity coefficient of the K-dV equation α_2 is controlled by the thickness of each layer and could be used to determine the shape of the resulting mode-2 ISW. Accordingly, the sign of the nonlinearity coefficient could be regarded as an index of the shape of the solitary wave in that environment. In the observations, similar approach could be made by examining α_2 with stratification in summer and winter, respectively. For the continuously stratified fluid, the variation of α_2 can be estimated using **Eqn.(9)** and **Eqn.(11)**. Where $W_2(z)$ and c_2 is estimated by **Eqn.(2)** and use the buoyancy frequency which is mentioned on section G in chapter II.

However, mode-1 ISWs became vague while mode-2 ISWs appeared frequently

in winter. It is interesting to examine the nonlinearity coefficient for mode-1 ISWs α_1 to figure out why mode-1 ISWs disappeared. Thus, α_1 is also calculated by the same method as estimating α_2 .

Fig.15A and **Fig.15B** shows comparison between the variations of the nonlinearity coefficients of the first two modes in summer and winter, respectively. **Fig.15A** is for summer. From top to bottom, the first panel is the depth contour of isotherms, the second panel is the contour of buoyancy frequency, and the third panel displays the variation of α_1 (red line) and α_2 (blue line), respectively. Each panel represents the same day, which is from 00:00 GMT, June 27 to 00:00 GMT, June 28. **Fig.15B** is similar as Fig.14A but for winter. From top to bottom, the first panel is the depth contour of isotherms, the second panel is the contour of buoyancy frequency, and the third panel displays the variation of α_1 (red line) and α_2 (blue line), respectively. Each panel represents the same day, which is from 00:00 GMT, December 21 to 00:00 GMT, December 22. Black rectangle indicates the mode-2 ISW.

In **Fig.15A**, the result shows that α_1 was always negative in summer, which agreed with the observations, depression mode-1 ISWs emerged twice each day in this mooring site. In addition, α_2 was often negative, too. It indicated that “concave type” mode-2 ISW might be dominant. However, no “concave type” mode-2 ISW was verified. According to observations, “usual” mode-2 ISWs were primary features in this period. Therefore, the stratification in summer could be unsuitable for the generation of “concave type” mode-2 ISW. As mentioned above, “usual” mode-2 ISWs could be related by the diurnal tide.

In **Fig.15B**, it indicated that α_2 was always positive while α_1 was close to zero in winter. From **Eqn.(9)**, the explanation for α_1 was nearly zero is that the phase speed c_1 could be nearly zero. It infers that there is no mode-1 ISW. Observations had also showed that mode-1 ISWs were vague. On the contrary, the positive α_2 corresponded to observations. “Usual” Mode-2 ISWs emerged frequently. The inference is that: as the thermocline became deep, the stratification or the so-called waveguide could be favorable for “usual” mode-2 ISWs but against mode-1 ISWs. Accordingly, those “usual” mode-2 ISWs could be locally generated under the stratification with a deep thermocline.

< D. Mode-2 ISW on satellite image >

Fig.16 is a MODIS image which was inside the sunlight area at 03:20 ~ 03:25 GMT, May 21, 2001. It is clear to see that there were signals revealing ISW packets with dark front lines and that a bright front line (**Fig.16**, red ellipse) was between two dark front lines. The signals with dark front lines are supposed to be depression mode-1 ISWs because the water is still deep in the northern area of Dong-Sha (Yang et al., 2004, Ramp et al., 2004). On the other hand, the bright front line could be considered a mode-1 elevation ISW. However, the elevation mode-1 ISW will not be generated if the water is deep. In theoretical considerations, the shape of the upper part of a mode-2 ISW is the same as an elevation mode-1 ISW. Accordingly, the bright front line could be a mode-2 ISW.



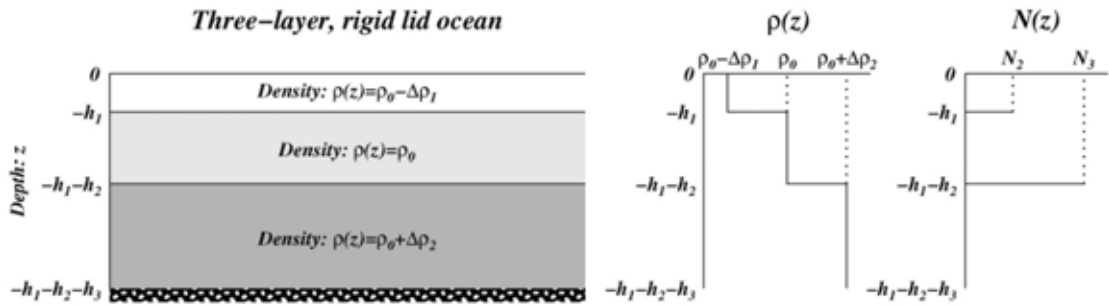


Fig.12 From left to right is the illustration of a 3-layer ocean, the distribution of density, and the distribution of BruntVaisalla frequency.

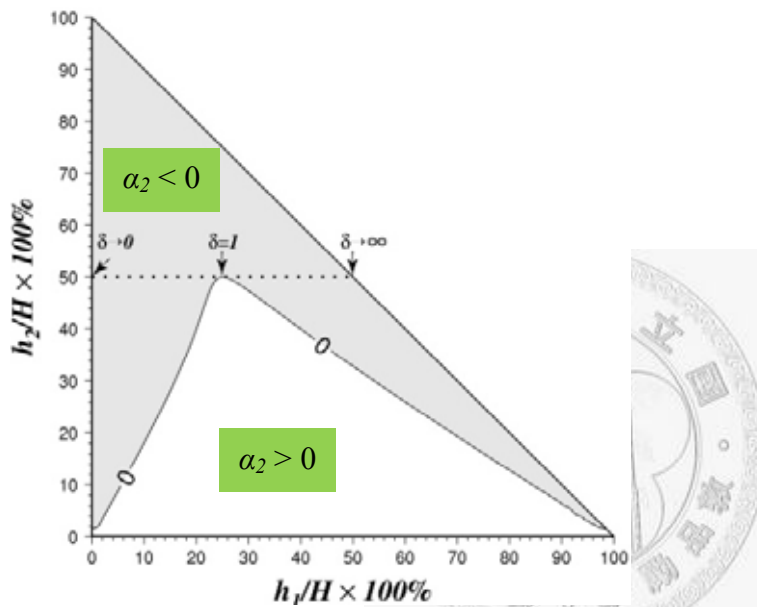


Fig.13 The region of $\alpha_2 > 0$ and $\alpha_2 < 0$ when $\Delta\rho_1 = \Delta\rho_2$ ($\delta=1$). The x axis represents the percentage of the thickness of the upper layer h_1 of the total water depth ($H=h_1+h_2+h_3$). The y axis represents the percentage of the thickness of the intermediate layer h_2 of the total water depth ($H=h_1+h_2+h_3$).



Fig.14 From left to right is the illustration of the mode-2 ISW (usual) and “concave type” mode-2 ISW.

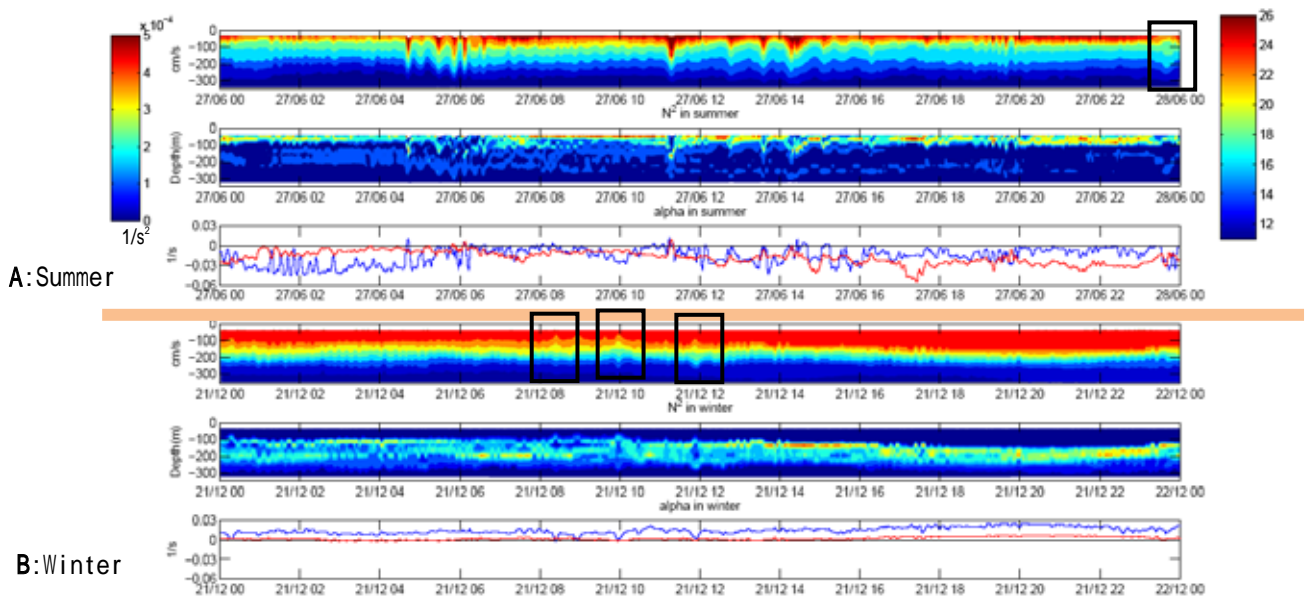


Fig.15 The comparison between the variations of the nonlinearity coefficient of the first two modes in summer and winter, respectively. **A**: From top to bottom, the first panel is the depth contour of isotherms, the second panel is the contour of buoyancy frequency, and the third panel displays the variation of α_1 (red line) and α_2 (blue line), respectively. Each panel represents the same day, which is from 00:00 GMT, June 27 to 00:00 GMT, June 28. **B**: From top to bottom, the first panel is the depth contour of isotherms, the second panel is the contour of buoyancy frequency, and the third panel displays the variation of α_1 (red line) and α_2 (blue line), respectively. Each panel represents the same day, which is from 00:00 GMT, December 21 to 00:00 GMT, December 22. Black rectangle indicates the mode-2 ISW.

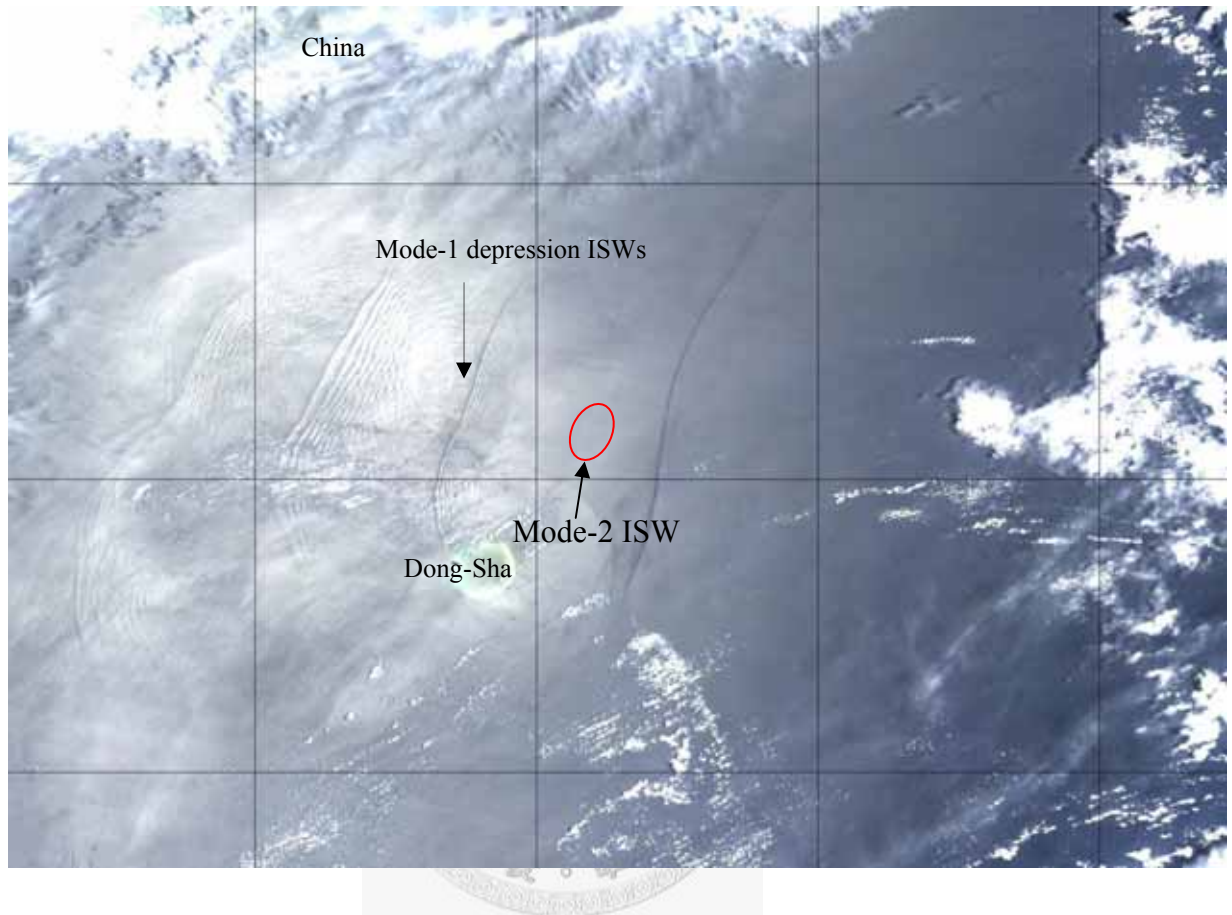


Fig.16 Satellite image (MODIS) captured a signal of mode-2 ISW (red ellipse) near Dong-Sha. (By courtesy of Yang)

IV. Conclusions

Using mooring observation of northern SCS, data collected by thermistor chain and an ADCP revealed a number of signals of mode-2 ISW. Typically, the mode-2 ISWs show the upward/downward displacement of isotherms in the upper/lower water column, respectively. According to previous studies, the modal displacement η_n can be governed by the K-dV equation. The displacement of isotherms and the characteristic time scale can be fitted by a square of the hyperbolic secant function. Accordingly, the displacement of isotherms induced by mode-2 ISWs are 33 ± 4 m and 28 ± 4 m in the upper and lower water column, respectively. The characteristic time scale is about 18 minutes as well as the maximum displacement of isotherms is ~ 80 m. The propagating direction of mode-2 ISWs is also studied. The westward propagating mode-2 ISW is prevailing and most mode-2 ISWs emerge during the neap tide period. In summer, mode-2 ISWs could have phase-locked with the diurnal tide about 24 hours. In winter, mode-2 ISWs emerge randomly but frequently. The seasonal difference could be associated with the vertical stratification variations. The buoyancy frequency in summer and winter show the thermocline is deep in winter. The analytic solution in the 3-layer ocean infers that a mode-2 ISW could exist in case the thickness of the intermediate layer is less than 50% of water depth. It is approximate to the stratification with a deep thermocline in winter. In addition, the sign of the nonlinearity coefficient of the K-dV equation α_n could be regarded as an index of the shape of the solitary wave in that environment. When $\alpha_1 > 0$, $\eta_1 > 0$ which is an elevation solitary wave. When $\alpha_1 < 0$, $\eta_1 < 0$ which is a depression solitary wave. In addition, in the mode-2 condition, when $\alpha_2 > 0$, it will be $\eta_2 > 0$ above the nodal point of the vertical velocity and $\eta_2 < 0$ below the nodal point. The shape of the wave is the same as the one observed in the northern SCS. The nonlinearity coefficient for the second mode is always positive in winter as the thermocline is deep. However, the nonlinearity coefficient for the first mode is close to zero, which means there could be no mode-1 ISWs. The result agrees with observations, mode-2 ISWs emerged frequently but mode-1 ISWs were vague. It is implicated that when the thermocline is deep, it is a waveguide which is favorable for the generation of mode-2 ISW but against mode-1 ISWs. Mode-2 ISWs could be generated locally in winter. However, the generating mechanism of mode-2 ISW is different in summer. It could be

associated with the diurnal tide. Future study is needed.

The primarily research limitation is that: the data is only form a single mooring. The phase speed of a mode-2 ISW cannot be estimated. The number of mounted thermistors could be not enough. If the resolution of data in vertically would be better as increasing the number of mounted thermistors, signals of other small amplitude mode-2 ISWs or “concave type” mode-2 ISW could be revealed more explicitly. Statistical result and the difference of mode-2 ISWs between summer and winter could be more precise and apparent.



Reference

Apel, J. R., M. Badiey, C. S. Chiu, S. Finette, R. Headrick, J. Kemp, J. R. Lynch, A. Newhall, M. H. Orr, B. H. Pasewark, D. Tielbuerger, K. von der Heydt, and S. Wolf (1997), "An overview of the 1995 SWARM shallow-water internal wave acoustic scattering experiment," *IEEE J. Ocean. Eng.*, vol. 22, pp. 465–500, 1997.

Apel, J. R. (2003), "A new analytical model for internal solitons in the ocean," *J. Phys. Oceanogr.*, Vol. 23, 2247-2269.

Baines, P. G. (1995), *Topographic Effects in Stratified Flows*, Cambridge University Press.

Batchelor, G. K. (1955), On steady laminar flow with closed streamlines at large Reynolds number, *J. Fluid Mech.*, Vol. 1, 177-191.

Beardsley, R. C., T. F. Duda, J. F. Lynch, S. R. Ramp, J. D. Irish, C.-S. Chiu, T. Y. Tang, and Y. J. Yang, "The barotropic tide in the northeast South China Sea," *IEEE J. Oceanic Eng.*, vol. 29, pp. 1075–1086, Oct. 2004.

Benjamin, T. B. (1967), Internal waves of permanent form in fluids of great depth, *J. Fluid Mech.*, Vol. 29, 559-592.

Chang, M. H. (2001), A study of Internal Solitons in the South China Sea. *Master Thesis*, Institute of Oceanography, College of Science, National Taiwan University.

Davis, R. E., and A. Acrivos (1967), Solitary internal waves in deep water, *J. Fluid Mech.*, Vol. 29, 593-607.

Duda, T. F., J. F. Lynch, J. D. Irish, R. C. Beardsley, S. R. Ramp, C.-S. Chiu, T. Y. Tang, and Y. J. Yang, "Internal tide and nonlinear internal wave behavior at the continental slope in the northern South China Sea," *IEEE J. Oceanic Eng.*, vol. 29, pp. 1105–1130, Oct. 2004.

Fu, L. L., and B. Holt (1982), Seasat views oceans and sea ice with synthetic aperture radar, *JPL Publications*, 81-120.

Gill, A. E (1982), *Atmosphere-Ocean Dynamics*. San Diego, CA: Academic.

Helfrich, K. R., and W. K. Melville (1986), On long nonlinear internal waves over slope-shelf topography, *J. Fluid Mech.*, Vol. 167, 285-308.

Helfrich, K. R (1992), Internal solitary wave breaking and run-up on a uniform slope, *J. Fluid Mech.*, Vol. 243, 133-154.

Lamb, K. G. (1994), Numerical experiments of internal wave generation by strong tidal flow across a finite amplitude bank edge, *J. Geophys. Res.*, Vol. 99, No. C1, 843-864.

Lamb, K. G., and B. Wan (1998), Conjugate flows and flat solitary waves for a continuously stratified fluid, *Phys. Fluids*, Vol 10, No. 8, 2061-2079.

Lee, C. Y., and R. C. Beardsley (1974), The generation of long nonlinear internal waves in a weakly stratified shear flow. *J. Geophys. Res.*, **79**, 453-457.

Liu, A. K., Y. Zhao, T. Y. Tang, and S. R. Ramp, "A case study of internal wave propagation during ASIAEX-2001," *IEEE J. Oceanic Eng.*, vol. 29, pp. 1144–1156, Oct. 2004.

Long, R. R (1953), Some aspects of the flow of stratified fluids. I. A theoretical investigation. *Tellus* **5**, 42.

Osborne, A. R., and T. L. Burch (1980), Internal solitons in the Andaman Sea, *Sci.*, Vol. 208, No. 4443, 451-590.

Ostrovsky, L. A., and Y. A. Stepanyants (1989), Do internal solitons exist in the ocean., *Rev. Geophys.*, 27, 293-310.

Ramp, S. R., Tang, T. Y., Duda, T. F., Lynch, J. F., Senior member, IEEE, Liu, A. K., Chiu, C. S., Bahr, F. L., Kim, H-R, and Y-J. Yang (2004), Internal Solitons in the Northeastern South China Sea Part I: Sources and Deep Water Propagation, *IEEE J. Ocean. Eng.*, Vol. 29, No. 4, 1157-1181.

Stamp, A. P., and M. Jacka (1995), Deep-water internal solitary waves, *J. Fluid Mech.*, Vol. 305, 347-371.

Stastna, M., and W. R. Peltier (2004), Upstream-propagating solitary waves and forced internal-wave breaking in stratified flow over a sill, *Proc. R. Soc. Lond. A*, **460**, 3159-3190.

Sutherland, B. R. (2002), Interfacial gravity currents. I. Mixing and entrainment, *Phys. Fluids*, Vol. 14, No. 7, 2244-2254, doi: 10.1063/1.1483303.

Tung, K. -K., Chan, T. F., and T. Kubota (1982), Large amplitude internal wave of permanent form, *Stud. Appl. Maths* **66**, 1-44.

Vlasenko, V. and K. Hutter (2001), Generation of second mode solitary waves by the interaction of a first mode soliton with a sill, *Nonlinear Proc. Geophys.*, **8**, 223-239.

Vlasenko, V, Stashchuk, N. and K. Hutter (2005), Baroclinic Tides – Theoretical Modeling and Observational Evidence, ch5, CAMBRIDGE UNIVERSITY PRESS.

Vlasenko, V., and W. Alpers (2005), Generation of secondary internal waves by the interaction of an internal solitary wave with an underwater bank, *J. Geophys. Res.*, **110**, C02019, doi:10.1029/2004JC002467.

Yang, Y. J., Tang, T. Y., Chang, M. H., Liu, A. K., Hsu, M-K., and S. R. Ramp (2004), Solitons Northeast of Tung-Sha Island During the ASIAEX Pilot Studies, *IEEE J. Ocean. Eng.*, Vol. 29, No. 4, 1182-1199.

Appendix

< The nonlinearity coefficient of the K-dV equation >

$$\frac{\partial \eta_n}{\partial t} + c_n \frac{\partial \eta_n}{\partial x} + \alpha_n \eta_n \frac{\partial \eta_n}{\partial x} + \beta_n \frac{\partial^3 \eta_n}{\partial x^3} = 0 \quad , \quad (\text{A})$$

η_n is the modal displacement, c_n is the linear phase speed of the wave, α_n is the nonlinearity coefficient, β_n is the dispersion coefficient. They are given by **Eqn.(9)**, **Eqn.(10)**, **Eqn.(11)**.

For a mode-1 ISW in a 2-layer system, assuming η_1 is the solution of (A), (A) can be written as:

$$\frac{\partial \eta_1}{\partial t} + c_1 \frac{\partial \eta_1}{\partial x} + \alpha_1 \eta_1 \frac{\partial \eta_1}{\partial x} + \beta \frac{\partial^3 \eta_1}{\partial x^3} = 0 \quad (\text{B})$$

If the sign of η_1 and α_1 are different, the solution of (A) would be η^* . (A) can be written as:

$$\begin{aligned} & \frac{\partial \eta^*}{\partial t} + c_1 \frac{\partial \eta^*}{\partial x} - \alpha_1 \eta^* \frac{\partial \eta^*}{\partial x} + \beta \frac{\partial^3 \eta^*}{\partial x^3} = 0 \\ \Rightarrow & -\frac{\partial(-\eta^*)}{\partial t} - c_1 \frac{\partial(-\eta^*)}{\partial x} - \alpha_1(-\eta^*) \frac{\partial(-\eta^*)}{\partial x} - \beta \frac{\partial^3(-\eta^*)}{\partial x^3} = 0 \\ \Rightarrow & \frac{\partial(-\eta^*)}{\partial t} + c_1 \frac{\partial(-\eta^*)}{\partial x} + \alpha_1(-\eta^*) \frac{\partial(-\eta^*)}{\partial x} + \beta \frac{\partial^3(-\eta^*)}{\partial x^3} = 0 \end{aligned} \quad (\text{C})$$

It can conclude that $\eta^* = -\eta_1$. Thus, in mode-1 condition, for $\alpha_1 > 0$, the displacement of the solitary wave, $\eta_1 > 0$ ($h_1 > h_2$), which is an elevation mode-1 ISW. For $\alpha_1 < 0$ ($h_1 < h_2$), the displacement of the solitary wave, $\eta_1 < 0$, which is a depression mode-1 ISW. Accordingly, in a 3-layer system, the degree of freedom of the internal motion is 2. In the mode-2 condition, when $\alpha_2 > 0$, it will be $\eta_2 > 0$ above the nodal point of the vertical velocity and $\eta_2 < 0$ below the nodal point. The other condition is When $\alpha_2 < 0$, it will be $\eta_2 < 0$ above the nodal point of the vertical velocity and $\eta_2 > 0$ below the nodal point.

< 3-layer ocean >

Assuming the ocean is a 3-layer fluid, the density of the upper layer is $\rho_0 - \Delta\rho_1$, the density of intermediate layer is ρ_0 , the density of the bottom layer is $\rho_0 + \Delta\rho_2$, using

rigid lid approximation (**Fig.12**), and define the buoyancy frequency N :

$$N(-h_1) = N_2 = \sqrt{\frac{g}{\rho_0} \frac{\Delta\rho_1}{\Delta z}}, \Delta z = h_1 \quad (\text{D-1})$$

$$N(-h_1 - h_2) = N_3 = \sqrt{\frac{g}{\rho_0} \frac{\Delta\rho_2}{\Delta z}}, \Delta z = h_2 \quad (\text{D-2})$$

The analytic solution can be derived by **Eqn.(2)** via boundary conditions: as follows:

(a) When $-h_1 - h_2 - h_3 \leq z < -h_1 - h_2$, $\rho(z) = \rho_0 + \Delta\rho_2$, which is a constant. It

concludes that $N(z) = 0$. (1)

(b) When $z = -h_1 - h_2$, assuming a perturbation with the vertical velocity W_4 at the interface, it has $W(-h_1 - h_2) = W_4$.

(c) When $-h_1 - h_2 < z < -h_1$, $\rho(z) = \rho_0$, which is a constant. It concludes that $N(z) = 0$.

(e) When $z = -h_1$, assuming a perturbation with the vertical velocity W_3 at the interface, it has $W(-h_1) = W_3$.

(f) When $-h_1 < z \leq 0$, $\rho(z) = \rho_0 - \Delta\rho_1$, which is a constant. It concludes that $N(z) = 0$.

The vertical structure of the vertical velocity can be written as:

$$W(z) = \begin{cases} -\frac{W_3}{h_1} z & -h_1 \leq z \leq 0 \\ \frac{W_3 - W_4}{h_2} (z + h_1 + h_2) + W_4 & -h_1 - h_2 \leq z \leq h_1 \\ \frac{W_4}{h_3} (z + h_1 + h_2 + h_3) & -h_1 - h_2 - h_3 \leq z \leq h_1 - h_2 \end{cases} \quad (\text{D-4})$$

The vertical structure of the horizontal velocity $U(z)$ can be derived by

$$U(z) = \frac{dW(z)}{dz} \quad (\text{D-5})$$

and:

$$U(z) = \begin{cases} -\frac{W_3}{h_1} & -h_1 \leq z \leq 0 \\ \frac{W_3 - W_4}{h_2} & -h_1 - h_2 \leq z \leq h_1 \\ \frac{W_4}{h_3} & -h_1 - h_2 - h_3 \leq z \leq h_1 - h_2 \end{cases} \quad (\text{D-6})$$

In order to derive the linear phase speed c , first, integrate **Eqn.(2)** from $z = -h_1 - \Delta z/2$ to $z = -h_1 + \Delta z/2$ and using (D-1), (D-5). Then, Integrate **Eqn.(2)** from $z = -h_1 - \Delta z/2$ to $z = -h_1 + \Delta z/2$ and using (D-2), (D-5), It has:

$$c^2 = \frac{g}{\rho_0} \frac{h_1(h_2 + h_3)\Delta\rho_1 + (h_1 + h_2)h_3\Delta\rho_2}{2(h_1 + h_2 + h_3)} \pm \frac{g}{\rho_0} \frac{\sqrt{[h_1(h_2 + h_3)\Delta\rho_1 + (h_1 + h_2)h_3\Delta\rho_2]^2 - 4(h_1 + h_2 + h_3)h_1h_2h_3\Delta\rho_1\Delta\rho_2}}{2(h_1 + h_2 + h_3)} \quad (\text{D-7})$$

It can see that (58) has two roots. It means that there are two linear phase speed. For convenience, one is named c_1 , the other is named c_2 . And define: $\delta = \Delta\rho_2/\Delta\rho_1$. It has:

$$c_1^2 = \frac{g}{\rho_0} \Delta\rho_1 \frac{h_1(h_2 + h_3) + (h_1 + h_2)h_3\delta}{2(h_1 + h_2 + h_3)} + \frac{g}{\rho_0} \Delta\rho_1 \frac{\sqrt{[h_1(h_2 + h_3) + (h_1 + h_2)h_3\delta]^2 - 4(h_1 + h_2 + h_3)h_1h_2h_3\delta}}{2(h_1 + h_2 + h_3)} \quad (\text{D-8})$$

$$c_2^2 = \frac{g}{\rho_0} \Delta\rho_1 \frac{h_1(h_2 + h_3) + (h_1 + h_2)h_3\delta}{2(h_1 + h_2 + h_3)} - \frac{g}{\rho_0} \Delta\rho_1 \frac{\sqrt{[h_1(h_2 + h_3) + (h_1 + h_2)h_3\delta]^2 - 4(h_1 + h_2 + h_3)h_1h_2h_3\delta}}{2(h_1 + h_2 + h_3)} \quad (\text{D-9})$$

For a right propagating wave, c_1 and c_2 must > 0 . And from (D-8) and (D-9), $c_1 > c_2$. c_1 can be regarded as the phase speed of the motion of mode-1 and c_2 can be regarded as the phase speed of the motion of mode-2.

For mode-2 case, W_3 and W_4 have the following relation:

$$W_4 = -\left(\frac{h_2}{c_2^2} \frac{g}{\rho_0} \Delta\rho_1 - \frac{h_2}{h_1} - 1\right)W_3 \quad (\text{D-10})$$

Define:

$$\gamma_2 = \frac{h_2}{c_2^2} \frac{g}{\rho_0} \Delta\rho_1 - \frac{h_2}{h_1} - 1 \quad (\text{D-11})$$

(D-11) can be written as:

$$W_4 = -\gamma_2 W_3 \quad (\text{D-12})$$

In general case, c_2 has the smaller value. So the first term on the right hand side in (D-11) will be larger. It concludes that $\gamma_2 > 0$ and the sign of W_4 and W_3 will be different. The solution of the motion of mode-2 can be derived from (D-4), (D-6) and by (D-12), it gets that:

$$W(z) = \begin{cases} -\frac{W_3}{h_1} z & -h_1 \leq z \leq 0 \\ \frac{1+\gamma_2}{h_2} (z+h_1+h_2)W_3 - \gamma_2 W_3 & -h_1-h_2 \leq z \leq h_1 \\ -\frac{\gamma_2}{h_3} (z+h_1+h_2+h_3)W_3 & -h_1-h_2-h_3 \leq z \leq h_1-h_2 \end{cases} \quad (\text{D-13})$$

$$U(z) = \begin{cases} -\frac{W_3}{h_1} & -h_1 \leq z \leq 0 \\ \frac{1+\gamma_2}{h_2} W_3 & -h_1-h_2 \leq z \leq h_1 \\ -\frac{\gamma_2}{h_3} W_3 & -h_1-h_2-h_3 \leq z \leq h_1-h_2 \end{cases} \quad (\text{D-14})$$

The nodal point of $W(z)$ is located at:

$$z = -h_1 - \frac{h_2}{1+\gamma_2} \quad (\text{D-15})$$

The solution of (D-13), (D-14) are shown in **Fig.17**, which agree with the numerical solution.

For mode-2 case, α_2 can be derived **Eqn.(9)**:

From **Eqn.(9)**, it has:

$$\alpha_2 = \frac{3c_2}{2} \frac{\left[\frac{(1+\gamma_2)^3}{h_2^2} - \frac{1}{h_1^2} - \frac{\gamma_2^3}{h_3^2} \right] W_3^3}{\left[\frac{(1+\gamma_2)^2}{h_2} + \frac{1}{h_1} + \frac{\gamma_2^2}{h_3} \right] W_3^2} = \frac{3c_2}{2} \frac{\frac{(1+\gamma_2)^3}{h_2^2} - \frac{1}{h_1^2} - \frac{\gamma_2^3}{h_3^2}}{\frac{(1+\gamma_2)^2}{h_2} + \frac{1}{h_1} + \frac{\gamma_2^2}{h_3}} W_3 \quad (\text{D-16})$$

Fig.13 shows the region of $\alpha_2 > 0$ and $\alpha_2 < 0$ when $\Delta\rho_1 = \Delta\rho_2$ ($\delta = 1$). The x axis represents the percentage of the thickness of the upper layer h_1 of the total water depth ($H=h_1+h_2+h_3$). The y axis represents the percentage of the thickness of the intermediate layer h_2 of the total water depth ($H=h_1+h_2+h_3$).

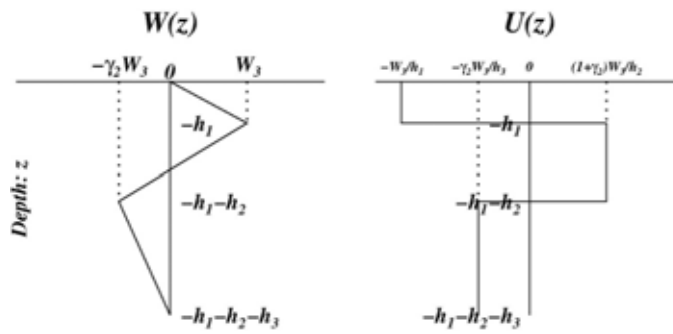


Fig.17 From left to right is the vertical structure of the vertical velocity and the vertical structure of the horizontal velocity for the motion of mode-2 in a 3-layer ocean.



